Two decades of flask observations of atmospheric δ(O₂/N₂), CO₂, and APO at stations Lutjewad (the Netherlands) and Mace Head (Ireland), and 3 years from Halley station (Antarctica)

Linh N.T. Nguyen[1], Harro A.J. Meijer[1], Charlotte van Leeuwen[1], Bert A.M. Kers[1], H.A. (Bert)
Scheeren[1], Anna E. Jones[2], Neil Brough[2,*], Thomas Barningham[2], Penelope A. Pickers[3], Andrew
C. Manning[3], and Ingrid T. Luijkx[4]

[1]Centre for Isotope Research, Energy and Sustainability Research Institute Groningen, University of Groningen,
Groningen, the Netherlands
[2]British Antarctic Survey, Natural Environment Research Council, Cambridge, United Kingdom
[3]Centre for Ocean and Atmospheric Sciences, School of Environmental Sciences, University of East Anglia, Norwich,
United Kingdom
[4]Meteorology and Air Quality, Wageningen University and Research, Wageningen, the Netherlands
*Now at National Institute of Water and Atmospheric Research, Wellington, New Zealand

Correspondence to: Linh N.T. Nguyen (n.t.l.nguyen@rug.nl)

Abstract. We present 20-year flask sample records of atmospheric CO_2, δ(O₂/N₂) and APO (Atmospheric Potential Oxygen) from the stations Lutjewad (the Netherlands) and Mace Head (Ireland), and a 3-year record from Halley Station (Antarctica). We include details of our calibration procedures and the stability of our calibration scale over time. The results of our inter-comparison involving gas cylinders from various research laboratories worldwide also show that our calibration is of high quality and compatible with the internationally-recognised Scripps O_2 scale. The measurement records from Lutjewad and Mace Head show similar long-term trends during the period 2002-2018 of 2.31 ± 0.07 ppm yr^{-1} for CO_2 and -21.2 ± 0.8 per meg yr^{-1} for δ(O₂/N₂) at Lutjewad, and 2.22 ± 0.04 ppm yr^{-1} for CO_2 and -21.3 ± 0.9 per meg yr^{-1} for δ(O₂/N₂) at Mace Head. They also show a similar δ(O₂/N₂) seasonal cycle with an amplitude of 54 ± 4 per meg at Lutjewad and 61 ± 5 per meg at Mace Head, while the CO_2 seasonal amplitude at Lutjewad (16.8 ± 0.5 ppm) is slightly higher than that at Mace Head (14.8 ± 0.3 ppm). We show that the observed long-term trends and seasonal cycles are compatible with the measurements from various other stations, especially the measurements from Weybourne Atmospheric Observatory (United Kingdom). However, there are remarkable differences in the progression of annual trends between the Mace Head and Lutjewad records for δ(O₂/N₂) and APO, which might in part be caused by sampling differences, but also by environmental effects, such as North Atlantic Ocean oxygen ventilation changes to which Mace Head is more sensitive. The Halley record shows clear trends and seasonality in δ(O₂/N₂) and APO, where especially APO agrees well with continuous measurements at the same location made by the University of East Anglia, while CO_2 and δ(O₂/N₂) present slight disagreements, most likely caused by small leakages during sampling. From our 2002-2018 records, we find good agreement for the global ocean carbon sink: 2.0 ± 0.8 PgC yr^{-1} and 2.2 ± 0.9 PgC yr^{-1}, based on Lutjewad and Mace Head, respectively. The data presented in this work are available at https://doi.org/10.18160/qq7d-t060 (Nguyen et al., 2021).

1 Introduction

The global carbon cycle is a dynamic system that comprises the exchanges of carbon between various reservoirs and is important for studying human-induced climate change and its impacts (Ciais et al., 2013). Accurate determination of anthropogenic CO_2 emissions and their partitioning across different reservoirs plays a vital role in understanding the impact of the remaining atmospheric CO_2 mole fraction on climate (Friedlingstein et al., 2020). High-precision atmospheric O_2 measurements have been proven to be a strong aide in quantifying CO_2 fluxes in the carbon cycle. By combining the decadal trends of atmospheric CO_2 and O_2, we can quantify the global land and ocean carbon sinks

(Bender et al., 1996; Keeling and Shertz, 1992; Manning and Keeling, 2006; Tohjima et al., 2019). This is because CO_2 and O_2 cycles are closely coupled – in most processes, there is an anti-correlation in the changes of their mole fraction, except for the oceanic uptake of CO_2 (Manning and Keeling, 2006). To quantify the various components of the global

45　carbon cycle, the changes in atmospheric mole fraction of the two species can be used in combination with their stoichiometric exchange ratio (ER), which is the ratio of CO_2 and O_2 exchanged (consumed/produced) in a process. The ER value varies depending on the process, and is close to 1.1 for photosynthesis/respiration (Severinghaus, 1995) and on average 1.38 for the global mix of fossil fuels (Keeling and Manning, 2014).

50　There are various techniques to measure atmospheric O_2 to high precision, such as interferometry (Keeling, 1988); mass spectrometry (Bender et al., 1994); paramagnetic analysis (Manning et al., 1999); gas chromatography (Tohjima, 2000); vacuum-UV absorption(Stephens et al., 2003; Stephens et al., 2021); and fuel cell technology (Stephens et al., 2007). Despite many improvements to these techniques over the years, it is still very challenging to obtain O_2 measurements with high accuracy and precision. This is mainly because the atmospheric background mole fraction of O_2 is very high

55　– around $209,392 \pm 3$ ppm (Tohjima, 2005) – while the observed variations are at the level of a few ppm. These challenges are magnified further for long-term measurements because of possible small biases, drifts or other changes in the analysers or in the calibration scales. Thus the sampling procedures and analysing (laboratory) conditions must be monitored and corrected for by a carefully designed use of calibration and reference gas cylinders over the years (Aoki et al., 2021). As a result, there are only a handful of programmes around the globe which are proficient in coupled

60　CO_2 and O_2 measurements, for example, the network of atmospheric stations maintained by the Scripps Institution of Oceanography (Manning and Keeling, 2006); National Institute of Advanced Industrial Science and Technology (Aoki et al., 2021); National Institute for Environmental Studies (Tohjima et al., 2008); University of East Anglia (UEA) (Pickers et al., 2017); and the University of Groningen (van der Laan-Luijkx et al., 2010). Our laboratory – the Centre for Isotope Research (CIO) of the University of Groningen (RUG) in the Netherlands – has been carrying out flask

65　measurements of CO_2 and O_2 since the early 2000s from various locations (van der Laan-Luijkx et al., 2010). Flask sampling for CO_2 and O_2 has been conducted at Lutjewad (the Netherlands), Mace Head (Ireland), Jungfraujoch (Switzerland) and Halley (Antarctica).

In this paper, we present the O_2 and CO_2 measurements from flasks collected at Lutjewad (the Netherlands), Mace Head

70　(Ireland), both for the period 2000-2020, and Halley (Antarctica) for 2014-2017. From these measurements, a tracer called Atmospheric Potential Oxygen (APO) (the details of which are given in Sect. 2.5) is calculated. We first describe the measurement sites and the sampling procedure as well as the measurement methods, including the calibration procedure. Then we present the data and discuss the trends and seasonality as well as the quality of the datasets. This paper builds on work previously presented in van der Laan-Luijkx et al. (2010), Sirignano et al. (2010), and van

75　Leeuwen (2015).

2 Methods

2.1 Site description

The stations from which our flasks were collected are: Lutjewad Atmospheric Monitoring Station on the northern coast of the Netherlands (53°24'N, 6°20'E) managed by the CIO (RUG); Mace Head Atmospheric Research Station on the

80　western coast of Ireland (53°20'N, 9°54'W) operated by the National University of Ireland's School of Physics and Ryan Institute Centre for Climate & Air Pollution studies; and (formerly) Halley VI Research Station situated on the

Brunt Ice Shelf (75°34′S, 25°30′W) operated by the British Antarctic Survey. Figure 1 shows the locations of the three stations.
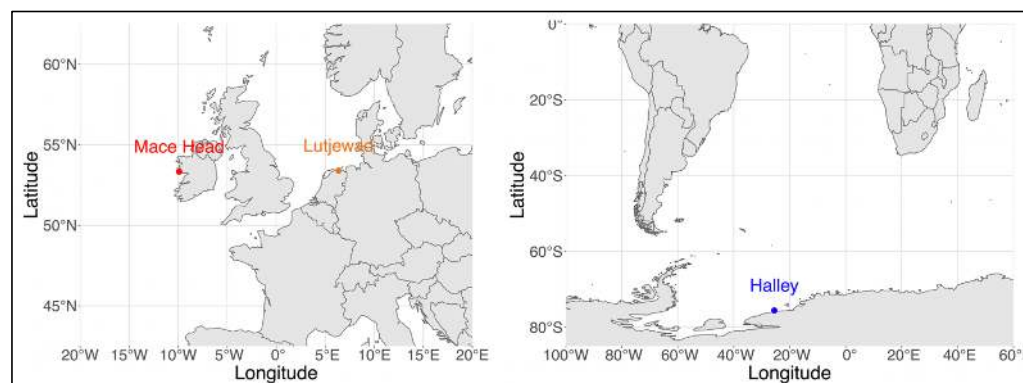
Figure 1: Left panel: Locations of the Mace Head (red) and Lutjewad (orange) stations. Right panel: Location of the Halley station (blue)

The Lutjewad station is a "class 2" station in the European Union's Integrated Carbon Observation System (ICOS) network. It comprises a 60-m tall tower, an additional platform of 10-m height, and a laboratory building containing analysers, flask sampling systems, measurement systems and other equipment. Air is pumped from the top of the 60-m tower via inlets connected to a series of tubing towards the laboratory building. The inlet is equipped with a Nafion drying tube (MD 110-72-S, Perma Pure, Toms River, New Jersey) so that the incoming air is first partly dried. The flow in the outer side of the Nafion tube is the outlet of the same air sampling system, after the air is dried with the second stage cryogenic dryer in the laboratory to a dewpoint below -45 °C (Neubert et al., 2004). This ensures that, except for water, all constituents have a negligible gradient over the Nafion membrane. From the inlet, the sampled air is stored in glass flasks via a flask sampling system for further analyses in the CIO laboratories (Neubert et al., 2004). The dominant wind direction in the Netherlands is southwest, meaning that the measurements acquired at the Lutjewad station often represent continental air masses influenced by anthropogenic and biogenic sources and sinks (van der Laan et al., 2010). Otherwise, when the wind comes from the north, the station samples background air that comes from the North Sea and North Atlantic (van der Laan-Luijkx et al., 2010).

The Mace Head station consists of field laboratories and a 20-m tower for sampling. The dominant wind arriving at the station is westerly from the North Atlantic Ocean, carrying air masses that would not have been considerably affected by regional anthropogenic activities. Air masses from other directions carry contamination from local and continental sources (Derwent et al., 2002; Jennings et al., 1993).

The Halley station is a "Global" station within the World Meteorological Organisation's Global Atmosphere Watch (WMO/GAW) programme, that observes background atmospheric conditions at various locations around the globe. The main Halley station consists of 8 modules that are atop ski-fitted hydraulic legs, within which are the research facilities and living quarters. Air sampling for this project was carried out at the Clean Air Sector Laboratory, which is located 1.5km from the main station in a location that receives minimal contamination from station activities (Jones et al., 2008). The predominant winds are from the east, bringing background air masses from the South Atlantic sector of the Southern Ocean (60%) or from the continental plateaux (30%). Westerly winds that have passed over the Weddell Sea gyre occur 10% of the time (Barningham, 2018; British Antarctic Survey, 2021).

2.2 Flask sampling procedure

At Lutjewad, we employ an automated flask sampling system, hereafter called the autosampler (Neubert et al., 2004). For storing air samples, we use 2.5-litre glass flasks capped with two high-vacuum valves (Louwers, Hapert, NL) sealed with Viton o-rings. Our autosampler is designed to connect to and fill up to 20 flasks without requiring user intervention, and we can remotely control the opening/closing of the flask valves (via custom-made electric motor actuators) and the filling of samples (via a series including a gas pump, flow controllers, and magnetic solenoid valves). The autosampler schedule is controlled via custom-made software (written in Delphi programming language), and carries out the sampling procedure automatically, but it can also be operated remotely using software such as VNC or TeamViewer when needed. A normal filling procedure starts with the air stream being cryogenically dried and flushed through a flask for at least an hour before filling the flask slowly so that the sample remains at atmospheric pressure (to prevent the sample from fractionation and differential permeation through the o-rings cause by a pressure gradient (Sturm et al., 2004)) and moving to the next flask. Individual flasks can be preserved at any time. Samples at Lutjewad are collected under various conditions and time frequencies, but in this paper we present only the data from flasks collected under local background conditions, defined by van der Laan-Luijkx et al. (2010) as flasks taken while the [222]Radon activity monitored at the station was less than 3 Bq m^{-3} and with a CO mole fraction of less than 200 ppb. This filtering procedure is applied to the dataset after the flasks are analysed.

At Mace Head, flasks are collected once or twice per week via a manually operated system as described by Conway et al. (1994), at 35 m above sea level and mostly during restricted baseline conditions (Bousquet et al., 1996). The filter to retain flasks with a CO mole fraction of less than 200 ppb is also applied for flask samples from Mace Head.

At Halley, flasks are collected once a week depending on the meteorological conditions, via a portable manual sampler. This consists of a KNF diaphragm pump (KNF N86), flowmeter, drying agent (magnesium perchlorate), 7 μm filter and 3 sampling flasks connected in concession. The air is sampled about 6 metres above the snow surface on the east side of the building via Synflex tubing connected to an aspirated inlet (the details of the aspirated inlet are as described by Blaine et al. (2006)). The system is flushed for about 45 minutes at a flow rate of 2.5 L min^{-1} at atmospheric pressure before each flask is manually closed. The collected samples are stored in insulated aluminium boxes at room temperature until their annual return to the UK on the Antarctic supply ship.

After sample collection, flasks from the three stations are transferred back to our laboratory in Groningen for analysis. Typically, the mole fractions of CH_4, CO, CO_2 and O_2 (reported as $\delta(O_2/N_2)$, see next section) are measured (van der Laan et al., 2009), and additional analyses such as stable isotopes (for example ^{13}C and [18]O in CO_2) and radiocarbon (^{14}C in CO_2) are also conducted when required (van der Laan et al., 2010).

2.3 CO_2 measurement

All flask samples are analysed on an Agilent HP6890N gas chromatograph equipped with a Flame Ionization Detector (referred to as HPGC) to determine the mole fractions of CO_2, CO and CH_4. The HPGC system has a set-up similar to the GC-systems described by Worthy et al. (2003) and van der Laan et al. (2009). All working standard mixtures (made from dried ambient air) that were used to calibrate the HPGC have been calibrated on the HPGC system at CIO against a suite of 5 primary standards linked to the World Meteorological Organization (WMO) X2007 scale with CO_2 ranging between 354 and 426 μmol mol^{-1} (ppm). These primary standards were provided by the Earth System Research Laboratory (ESRL) of the National Oceanic and Atmospheric Administration (NOAA), USA. Since the summer of 2013, working standard gas cylinders were also calibrated for CO_2, CO and CH_4 mole fractions on a Cavity Ring-Down

Spectrometer (CRDS) model G2401-m from Picarro Inc. using the same suite of primary standards. We refer to Chen et al. (2010) for more details on the CDRS technique. The measurement precision and accuracy for flask measurements of CO_2 on the HPGC are typically <0.06 ppm and <0.07 ppm, respectively (van Leeuwen, 2015).

160

All CO_2 measurements presented in this paper were originally calibrated against standards on the WMO X2007 scale, and are updated to the WMO X2019 scale (the new scale is explained in details by Hall et al. (2020)).

2.4 O_2 measurements

Atmospheric O_2 is typically reported as the $\delta(O_2/N_2)$ value. The $\delta(O_2/N_2)$ value of a sample is calculated as the
165   difference between the O_2/N_2 ratio of the sample and that of a reference gas (Keeling and Shertz, 1992):

$$\delta(O_2/N_2) = \frac{(O_2/N_2)_{sample} - (O_2/N_2)_{reference}}{(O_2/N_2)_{reference}} \qquad (1)$$

Since for natural variations, $\delta(O_2/N_2)$ values are very small, they are usually expressed in "per meg", which is 1/1000 of a per mil, as typically used in the stable isotope community. Atmospheric O_2 is reported as O_2/N_2 ratio because it is not a trace gas, and its mole fraction is thus affected by changes in other atmospheric constituents such as CO_2.
170   Atmospheric N_2 is relatively very stable (Keeling et al., 1998), therefore changes in the O_2/N_2 ratio would reflect mostly the changes in atmospheric O_2 (only in a detailed budget analysis minor N_2 variabilities are still considered, as described in Keeling and Manning (2014)). For $\delta(O_2/N_2)$ measurements, we use a Micromass Optima Dual Inlet Isotope Ratio Mass Spectrometer (DI-IRMS). The DI-IRMS analytical technique (which was first developed by Bender et al. (1994)) follows the principles as explained by Keeling et al. (2004). Due to the sensitivity of the analyser, it is located inside a
175   climate-controlled room in our CIO laboratory, however the measurements still inevitably drift over time. To correct for the instrumental drifts, we perform frequent calibrations using a suite of reference gas cylinders. These cylinders are calibrated against the international Scripps scale using three primary standard cylinders purchased from the Scripps Institution of Oceanography (SIO), with $\delta(O_2/N_2)$ values ranging from -792 to -254 per meg. Details of the extensive calibration procedure are thoroughly described by van der Laan-Luijkx (2010) and van der Laan-Luijkx et al. (2010),
180   and are summarised in Sect. 3.

2.5 Atmospheric Potential Oxygen (APO)

Combining highly precise measurements of atmospheric CO_2 and O_2 can isolate the effects of the oceanic processes, by removing the effects of the land biosphere (Stephens et al., 1998). This is achieved by deriving the tracer Atmospheric Potential Oxygen (APO). The APO value of an air sample is determined by combining its $\delta(O_2/N_2)$ and
185   CO_2 measurements (Battle et al., 2006; Gruber et al., 2001; Stephens et al., 1998):

$$\delta APO = \delta(O_2/N_2) + \frac{1.1 \times (CO_2 - 350)}{S_{O_2}} \qquad (2)$$

The value of 1.1 represents the mean O_2:CO_2 ER of terrestrial ecosystems (Severinghaus, 1995); for the S_{O_2}, we take 0.2094, which is the standard atmospheric O_2 mole fraction (Tohjima, 2005); and 350 is the consensus (arbitrary) reference value to be subtracted from the measured CO_2 mole fraction, as defined in the SIO per meg scale conversion
190   for APO (Manning and Keeling, 2006). Therefore, APO is not affected by land biosphere processes and mainly captures the seasonal and long-term air-sea exchange of CO_2 and O_2, with a small influence from fossil fuels combustion, caused by their higher average ER of $\approx$1.4 (Pickers et al., 2017; Sirignano et al., 2010).

3 Calibration of the DI-IRMS

195 In this section we present the calibration procedure and the stability achieved at our laboratory from 2006 to 2020. The calibration of the measurements made in the 2000-2011 period and reported by van der Laan-Luijkx et al. (2010) and (van der Laan-Luijkx et al., 2013) are kept intact, and the newly calibrated measurements from 2011 onwards are built on the principles of that work.

3.1 The calibration procedure

200 The DI-IRMS compares the measurement of a sample gas with that of a reference gas (hereby called "machine reference" or "MREF") in a sequence of several switches back and forth ("change overs"). The result of this process is the $\delta(O_2/N_2)$ value of the sample, as presented in equation 1. Each individual measurement is based on seven successive pairs of sample and reference measurements, which are used to calculate seven delta values (equation 1). The seven delta values then go through a filtering process. First, the mean and standard deviation of the seven delta values are

205 calculated. Then, the delta value that is furthest from the mean is marked as a potential outlier. Next, a new mean and a new standard deviation are calculated for the remaining six delta values. If the excluded delta value is more than 2.7 times (equivalent to p = 0.01) the new standard deviation away from the new mean, it is defined as an outlier and removed. This process is repeated to identify and remove a potential second outlier (at most two outliers are removed by this process, otherwise the reliability of the measurement is sacrificed). After removing possible outliers, the

210 remaining delta values are averaged to produce one $\delta(O_2/N_2)$ value per measurement. A flask is typically measured two to three times consecutively, and the final measurement for each flask (as presented in this paper) is the average of the filtered $\delta(O_2/N_2)$ values of these repeated measurements (van der Laan-Luijkx et al., 2010).

To improve the stability of our measurements, we also measure local reference gas cylinders (hereafter called "working

215 tank" or "WT") on the sample side of the DI-IRMS. These WTs are also used to connect between periods of different MREF cylinders, where there may be shifts in the scales of the measurements and thus a scale conversion is required to keep all raw measurements on a comparable scale. The summary of different WTs and MREF cylinders used from 1998 to 2020 is shown in Fig. 2 and Table 1.
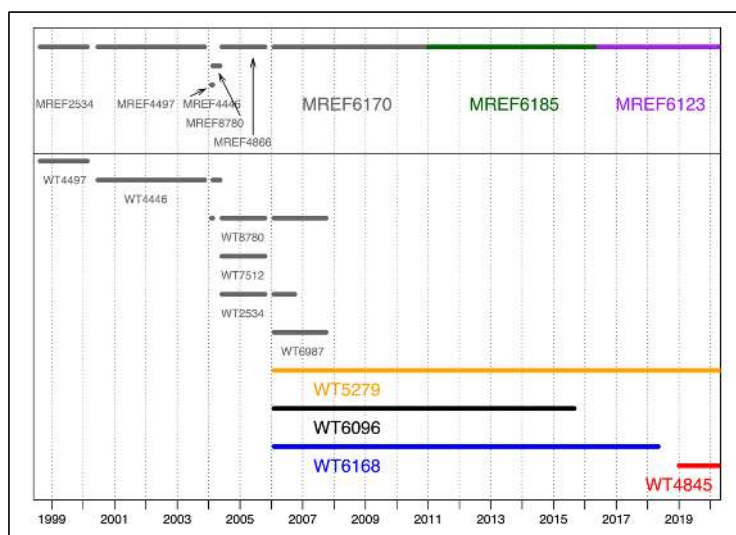
220 **Figure 2: Summary of the different WTs and MREF cylinders in the 1998 - 2020 period. MREFs are shown along the top, with WTs below. In the case of WTs, there is typically overlap between more than one WT.Periods in grey colour are adapted from the work of van der Laan-Luijkx (2010).**

To connect the different MREF periods, we first convert all raw measurements (which are the ratios of the raw values to their respective MREF) to our internal 2534 CIO scale. Subsequently, they are converted to the SIO scale. Cylinder

225   number 2534 has been chosen as the baseline for our internal reference scale, because it was the first MREF gas in 1998 and later on was measured as a WT against several other MREF cylinders (Fig. 2). When converting the measurements to the internal CIO scale, we need to take into account the "zero-enrichment" factor: measurements of a WT (on the sample side) against an MREF cylinder (on the reference side) do not produce the same value as when they are measured the other way around (van der Laan-Luijkx et al., 2010).

230

In addition to the conversion to our internal CIO scale, the measurements are also affected by instrumental drifts over time. To correct for these drifts, we first divide our long measurement record into several periods, which are defined based on the timing of when the MREF cylinders are changed, and/or apparent fluctuations in the raw data related to, for example, repairs or modifications of the system. In this work, the calibration procedure is carried out for

235   measurements from 2011 onwards, which were divided into seven periods (periods 9-15, Table 1).

Table 1: Summary of the calibration periods defined in this paper and the corresponding MREF cylinder and WT cylinder numbers most recently used for the calibration of the DI-IRMS.

	Period		MREF	WTs
Previous	1	17-08-1998 – 18-02-2000	2534	4497
	2	19-06-2000 – 17-11-2003	4497	4446
	3	03-02-2004 – 18-02-2004	4446	8780
	4	18-02-2004 – 14-05-2004	8780	4446
	5	04-06-2004 – 19-10-2005	4866	2534 | 7512 | 8780
	6	30-01-2006 – 30-12-2006	6170	2534 | 6987
	7	30-01-2007 – 30-12-2007	6170	5279| 6096 6168 | 6987
	8	30-01-2008 – 15-12-2010	6170	5279 | 6096 | 6168
Current	9	03-01-2011 – 11-03-2014	6185	5279 | 6096 | 6168
	10	11-03-2014 – 29-08-2015		5279 | 6096 | 6168
	11	30-08-2015 – 10-06-2016		5279 | 6168
	12	11-06-2016 – 05-05-2018	6123	5279 | 6168
	13	06-05-2018 – 01-01-2019		5279
	14	02-01-2019 – 11-03-2020		5279 | 4845
	15	12-03-2020 to present		5279 | 4845

These 7 periods were divided into 144 sub-periods (selected based on breaks in the records) which were then

240   individually processed to derive the final corrections for all measurements in those sub-periods. The complete step in transforming the raw measurements of a sample (S) against a current MREF (M) into comparable data is to combine the drift correction with the shift to the CIO scale (R), by using an equation described by van der Laan-Luijkx (2010):
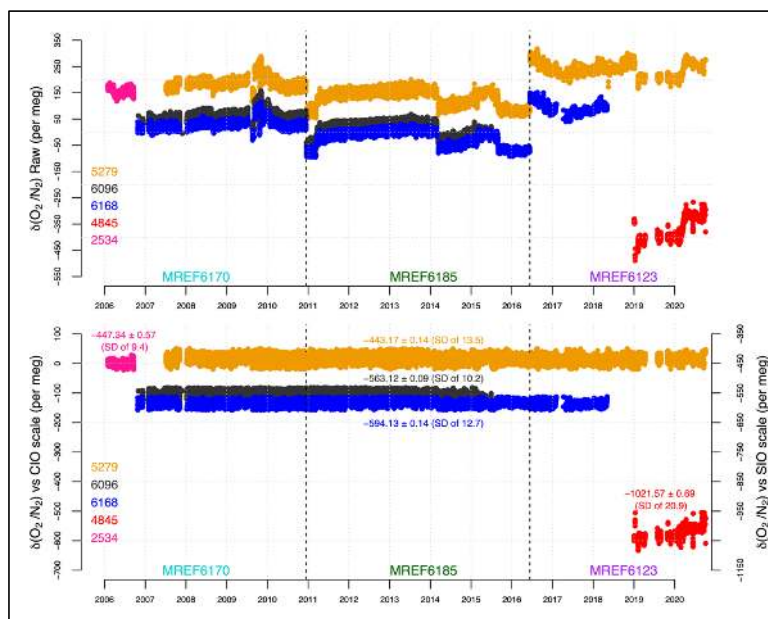
$$\delta_{S/R} = \left(\left(\delta_{M/R} \right)_{sub-period} + drift \times \frac{days}{365} + 1 \right) \times \left(\delta_{S/M} + 1 \right) - 1 \qquad (3)$$

Where:

245   - $\delta_{S/R}$ is the $\delta(O_2/N_2)$ value of the sample against the CIO 2534 scale;
-   $(\delta_{M/R})_{sub-period}$ is the average $\delta(O_2/N_2)$ value of the MREF cylinder against the CIO scale in a sub-period calculated based on the measurements of all WTs in that sub-period;
-   drift is the average drift per day in a sub-period (if any), calculated based on the WT values and days is the number of days at the time of the sample since the start of the sub-period.

250   - $\delta_{S/M}$ is the $\delta(O_2/N_2)$ value of sample against the MREF cylinder (raw value).

The final step is to transform the $\delta_{S/R}$ value of a sample onto the SIO scale via a linear conversion using the values of the Scripps primary cylinders measured against the CIO scale. For an extensive and detailed explanation on how to calculate each component of equation 3 and conversion to the SIO scale, we refer to van der Laan-Luijkx (2010). Figure

255   3 shows the results for the WTs of the new calibration procedure connected to the previously reported data by van der Laan-Luijkx et al. (2010).

Figure 3: Measurements of the 3 long-term WTs (5279, 6096, and 6168) for periods 7-15 (Table 1), across the final 3 MREF periods plus a recently added WT (4845). Top panel: raw measurements of the WTs against different MREF cylinders.
260   **Bottom panel: measurements of the WTs calibrated and converted to the CIO scale (left y-axis) and against the SIO scale (right y-axis). The values on the plot are the corresponding long-term means and 1-sigma standard errors of the WTs against the SIO scale, and in parentheses are the respective standard deviations. All numbers are in per meg. Visible gaps in the data are due to instrument issues, maintenance or instrument relocation.**

After these adjustments, the measurements of the 3 long-term WTs (5279, 6096, and 6168) show that they were
265   relatively stable over time, all showing standard deviations of 10.2 to 13.5 per meg (corresponding to standard errors of 0.09 to 0.14 per meg) over the 20-year period. WT 4845 was recently measured for a relatively short period only, and appears to be less stable and noisier compared to WT 5279 measured in the same period. Thus, WT4845 was not used for the calculations in the calibration procedure, and its measurements are only shown here for completeness.

270   In addition to their long-term stability, the 3 WTs also showed no systematic drifts across different MREF periods (Table 2). For WT 5279 and WT 6096, there are no significant changes (at least to ±0.3 per meg) between the MREF periods 6170 and 6185, although there is a small decrease of 4.0 per meg in the mean measurement of WT 5279 in MREF 6123 period. For WT 6168, the mean value increased by 3.6 per meg from MREF 6170 to MREF 6185 period, then dropped slightly (by 0.5 per meg) in MREF 6123 period. The stability demonstrated in both long-term
275   measurements and per MREF periods consolidates the quality of our calibration procedure.

280 **Table 2: Comparison of the WTs over 3 different MREF cylinder periods. The values (in per meg) are averaged over the corresponding period, accompanied by the standard errors. The N/A values in the MREF6123 period for WT6096 are due to its discontinuation in this period. The Difference column is calculated by subtracting the values of the old MREF periods from the new ones**

		CIO scale	SIO scale	Difference (CIO scale)
	MREF 6170	20.9 ± 0.2	-438.2 ± 0.2	
WT 5279	MREF 6185	20.7 ± 0.3	-438.4 ± 0.2	-0.2
	MREF 6123	16.7 ± 0.2	-442.3 ± 0.2	-4.0
	MREF 6170	-103.4 ± 0.1	-556.9 ± 0.1	
WT 6096	MREF 6185	-103.1 ± 0.1	-556.7 ± 0.1	+0.3
	MREF 6123	N/A	N/A	
	MREF 6170	-137.3 ± 0.2	-589.3 ± 0.2	
WT 6168	MREF 6185	-133.7 ± 0.2	-585.9 ± 0.2	+3.6
	MREF 6123	-134.2 ± 0.4	-586.4 ± 0.3	-0.5

3.2 Quality check of the Scripps primary cylinders

285 The final check on the quality of our scale is the regular measurement of the 3 Scripps primary standard cylinders that we purchased from SIO, numbered 7002, 7003, and 7008. These measurements were conducted at least once a year or when there was an additional need for recalibrating e.g. after instrument failure or upgrade. Each measurement period took a different amount of time – some measurements were spread over a couple of days while others were repeated over (or after) a few weeks. From 2007 to 2018, 16 measurement periods were conducted (Fig. 4). The large gap

290 between 2011 and 2014 was due to a lack of funding.

In Figure 4, each data point is the mean value over each measurement period and the error bars are the standard deviations. The coloured lines are the overall linear fit of the measured values of the corresponding cylinders (and their associated 2-sigma uncertainties) and the black horizontal lines are the assigned values of the cylinders (determined by

295 the SIO, updated in 2020). The assigned and measured values of the primary standard cylinders over the whole period are compared in Table 3. The measured values are the weighted means of each cylinder, since each data point is calculated based on different numbers of separate measurements. It can be seen from Figure 4 and Table 3 that cylinder 7008 exhibits a small upward drift over time of 1.4 ± 0.4 per meg yr^{-1}, whereas the other two remain constant. The ensemble thus suggests that there is no clear systematic error in our scale conversion and calibration procedure. To

300 improve the quality of our conversion into the SIO scale, and especially to check the behaviour of cylinder 7008, we are planning to purchase new primary standard cylinders in the future.

The conversion of the CIO scale to the Scripps scale is done using these measurements, and in such a way that the ensemble difference between the assigned values and weighted averages of our measurements of three Scripps cylinders

305 is minimised.
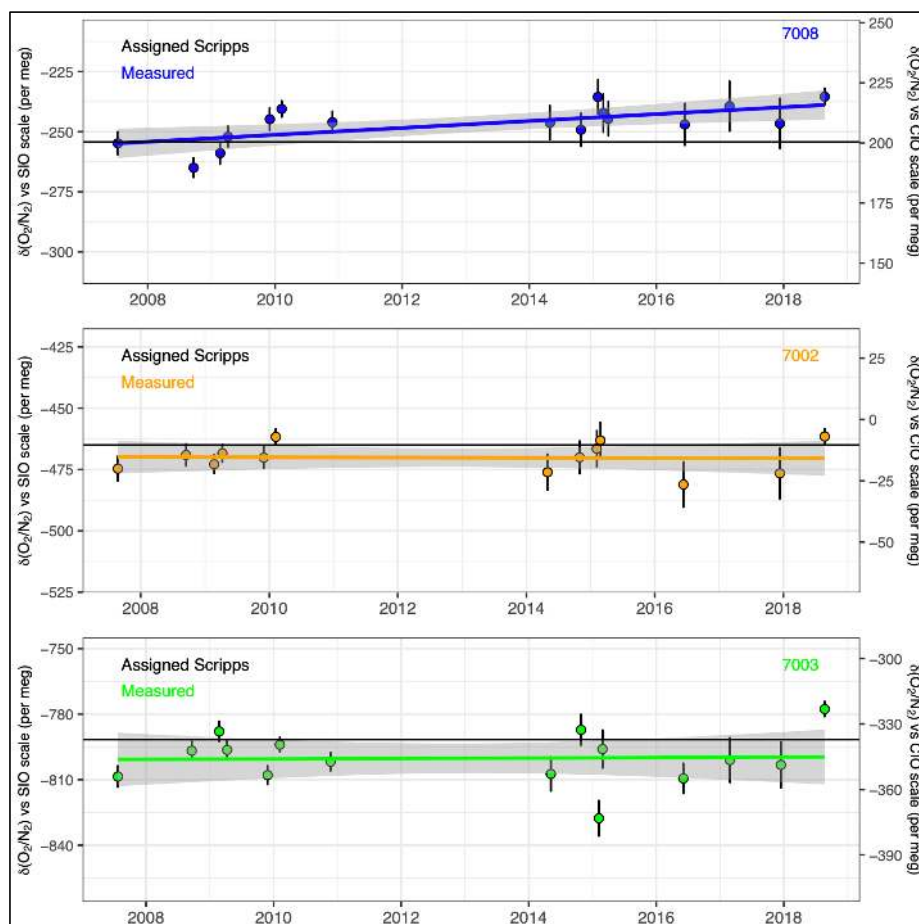
Figure 4: Scripps primary standard cylinder measurements over time. Each point is the averaged value over a measurement period. Error bars represent 1-sigma standard deviations. Solid horizontal lines are the assigned values (black) and the linear least squares fit to the data (coloured) of each cylinder. The grey shading indicates the 95%
310 **confidence interval uncertainties of the values.**

Table 3: Comparison of the averaged measured values of the Scripps primary standards against their assigned values in per meg.

Cylinder ID	7008	7002	7003
Assigned by SIO	-254.3	-465.0	-791.6
Weighted mean measured	-245.9	-468.9	-797.6
Standard deviation	8.0	6.0	11.8
Standard Error	1.9	2.0	2.8
Deviation from assigned	8.4	-3.9	-6.0

3.3 Inter-comparison programmes

In addition to measuring the primary standard cylinders, the CIO also took part in two inter-comparison programmes
315 involving oxygen measurements: "Cucumber" Intercomparison which was initialised in the European Union's CarboEurope project and coordinated by the UEA (http://cucumbers.uea.ac.uk/); and the Global Oxygen Laboratories Link Ultra-precise Measurements (GOLLUM) programme, also coordinated by UEA (Gollum Comparison: Manning et al., 2015) . These inter-comparison programmes provide an additional tool for checking the internal stability of our measurements, while also linking the oxygen measurements between global laboratories.

320   The Cucumber programme involves inter-comparison of nine atmospheric species (of which $\delta(O_2/N_2)$ is one) between
       atmospheric research stations in Europe and a number of laboratories in Europe, USA, Canada, Japan, and Australia.
       Within the programme, there are seven sets of three cylinders sent around in different rotations. The CIO participated
       in three rotations, with two involving oxygen measurements (called "Inter-1" and "Euro-3") (University of East Anglia,
       2021).

325

       The GOLLUM programme is specifically designed for the inter-comparison of oxygen measurements and involves 10
       laboratories worldwide that carry out high-precision atmospheric oxygen measurements. Two sets (named "Bilbo" and
       "Frodo") of three cylinders are rotated in opposite directions amongst participating laboratories (Gollum Comparison:
       Manning et al., 2015).

330

       Figure 5 shows the measurements of the Cucumber cylinders (top two panels), the cylinders in the Bilbo and Frodo
       rotations of GOLLUM (third and fourth panels, respectively) and the measurements of three internal cylinders at CIO:
       the working tanks 5279, 6096 and 6168 along with the SIO primary standard cylinder 7008 (bottom panel). The
       measurements of the cylinders in the Inter-1 and Euro-3 rotations are plotted as the difference between the measured
335   values of the cylinders against their own assigned values as originally measured at the Max Planck Institute for
       Biogeochemistry in Germany in January 2008. These results show that the cylinders in the Inter-1 and Euro-3 rotations
       were quite variable over time (varying within a range of less than 30 per meg) but in different directions and size,
       suggesting that there is not a systematic scaling error but rather individual variations between cylinders and/or
       measurement periods. Due to the individual variations, the overall drifts for Cucumber cylinders is 11 ± 18 per meg yr
340   [-1], higher than the WMO extended compatibility goal of 10 per meg (World Meteorological Organization, 2018). The
       lower quality of the measurements (not only in our laboratory) might well be connected to the fact that these cylinders
       are not part of a dedicated oxygen comparison programme, so the treatment of the cylinders (for example, vertical
       storage and unsuitable pressure reducers) are not of high enough standard for oxygen.

345   For GOLLUM cylinders, all measurements are also plotted as the difference between the measured values of the
       cylinders and their assigned values on the SIO scale. The assigned values for Bilbo, Frodo and SIO cylinders are
       determined at the SIO, while those for the WTs are their averaged long-term value measured at CIO on the SIO scale.
       Compared to the Cucumber cylinders, GOLLUM cylinders show much less variations between years (varying within a
       range of less than 20 per meg), and also significantly smaller overall drift over the duration of the measurements (4 ± 6
350   per meg yr^{-1}, which is within the extended WMO compatibility goal). However, all 6 cylinders appear to drift in similar
       direction, suggesting a drift (however small) in our scale rather than drifts in these cylinders. The SIO cylinder 7008
       also shows similar stability and a general drift in the same direction as GOLLUM cylinders, whereas the two other SIO
       cylinder do not (Fig. 4).

355   Since the cylinders show an inconclusive "drift": INTER-1 and EURO-3 do not show an apparent drift direction; Bilbo
       and Frodo present a minor drift similarly to that observed by our SIO cylinder 7008 (while the other 2 SIO cylinders
       did not exhibit this behaviour as shown in Sect. 3.2); and our internal WTs all show no overall drifts, we consider our
       calibration procedure as sufficient. Recalibration of the SIO cylinders might shed further light on these small
       discrepancies, mostly to see if cylinder 7008 has indeed drifted or not.
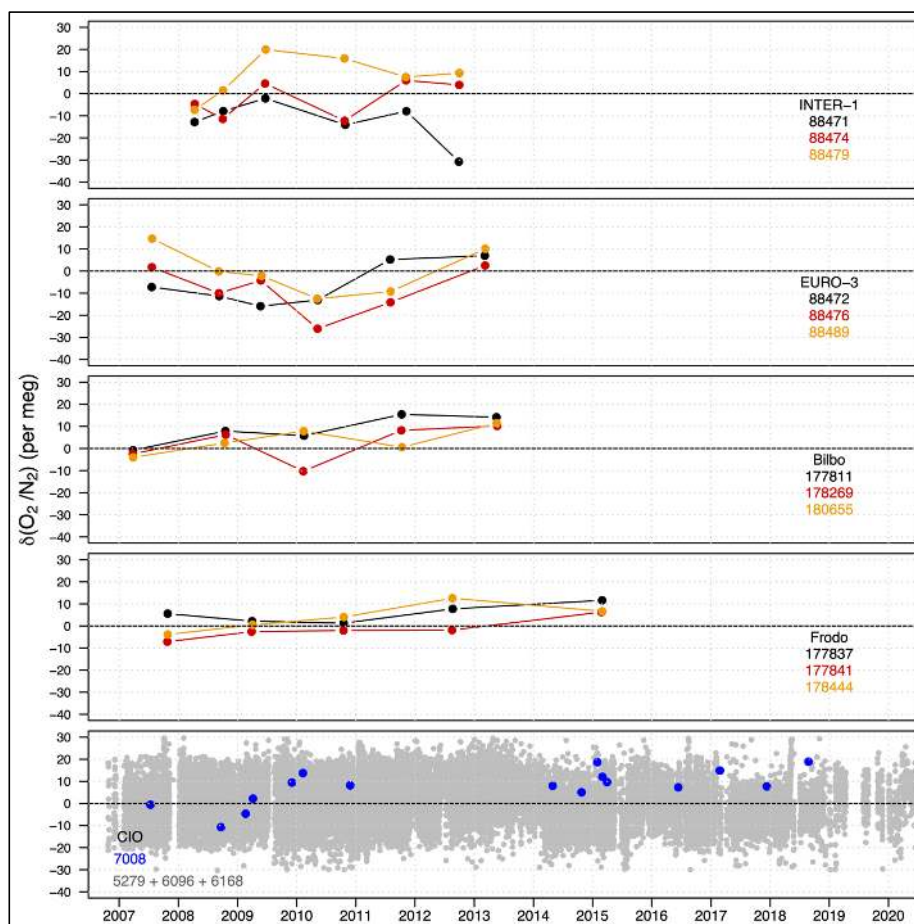
360

Figure 5: Cylinders from the Cucumber programme (top 2 panels) along with two sets of three cylinders in the GOLLUM programme (middle 2 panels) and 3 internal CIO cylinders (WT 5279, WT 6096 and WT 6168) and a primary standard cylinder at CIO (SIO 7008) (bottom panel). Each colour represents a different cylinder, and the legends show the corresponding cylinder IDs. The points are the measurements of the cylinders over time, plotted as the difference from
365 **their assigned values. For the Cucumber, GOLLUM and SIO cylinders, the assigned values are determined at the SIO, and for the WTs, the assigned value is its long-term average measured at CIO on the SIO scale. Y-axis ranges are identical on all panels.**

3.4 Treatment of analysed flask samples

After the calibration and conversion to the SIO scale, the individual flask sample measurements are scrutinized for
370 outliers and background conditions. For this purpose, we perform several iterations of fitting a combination of quadratic and 3-harmonic regression (following similar curve fitting methods applied to time series in NOAA (Thoning et al., 1989)) and filtering the outliers from the combined fit. This outlier filtering process uses the robust median absolute deviation (MAD) method (Rousseeuw and Verboven, 2002), in which the MAD value for a dataset is determined by first finding the median of the set, then subtracting the median from each individual value, and finally finding the
375 median of the absolute differences. Measurements that are 3 times the MAD value away from the median of the measurement set are considered outliers and removed. The full principle of the procedure is described by van der Laan-Luijkx (2010) (though with a different filtering process that was described in Sect. 3.1). In total, after both filtering processes, around 30% of the flasks were excluded from further analyses from Lutjewad samples, 16% from Mace Head samples, and only 6% from Halley samples. The larger fraction of discarded measurements in the Lutjewad record

380 is related to the sampling process, where we do not specifically only sample air at background conditions, which is the case at Mace Head. For Halley, since it is by design a background station, there are hardly any local sources and sinks, and the wind coming from the continental plateaux only accounts for 30% of the total. The 6% outlier fraction for Halley is a good indication of the fraction of actually failed sampling and/or analysis. The APO values of all stations are calculated from $\delta(O_2/N_2)$ and CO_2 measurements (equation 2), when there is information on both species for each

385 flask sample.

In the period prior to 2006, our internal calibration scale was not as well-established as in the later period, due to frequent changes in MREF and WT cylinders, especially in 2004 when there is little information to connect the following period to the first period (as presented in Fig. 2 and Table 1). Next to this, we also only obtained the SIO

390 primary standards in late 2007, so all earlier measurements cannot be directly linked to the SIO scale and have to be converted via the internal CIO scale. The results of this quality check prompt us to exclude the first 2 years from the fits of Lutjewad and Mace Head data so that they are less affected by the problematic period. The last 2 years are also excluded because flask sampling was relatively sparse in those years and this could also introduce biases in the fits. After several tests, we decided to establish our fits for Lutjewad and Mace Head based on the years 2002 to 2018.

395 **4 Flask measurement results**

4.1 The CO_2, $\delta(O_2/N_2)$ and APO records

In this section, we present the long-term flask measurement records (from 2000 to 2020) of Lutjewad and Mace Head, along with a 3-year record from Halley. In general, Lutjewad and Mace Head show similar patterns for $\delta(O_2/N_2)$ and CO_2, with some differences in APO variations. Figures 6 to 8 show the CO_2, $\delta(O_2/N_2)$, and APO measurements for

400 Lutjewad, Mace Head, and Halley, respectively. The black points illustrate the final, filtered flask measurement values; the coloured lines are the total fit (combined quadratic trend and 3-harmonic seasonal cycles) and the black lines are the trend parts of the total fit. The fit lines are shown for the whole period, but for the fitting process we left the first and last two years out, to make sure that the fit period comprises an exact multitude of years. Otherwise, the beginning and end of the curves can influence the trend part of the fit due to the irregular sampling frequency, as explained in

405 Sect. 3.4.

CO_2 measurements at Lutjewad and Mace Head show a positive, and increasing trend over 20 years. Due to the quadratic trend fit, the growth of the fitted increase is linear. The trend (given here in ppm yr^{-1} with their 95% confidence interval (CI) uncertainties) in Lutjewad grows from 1.81 ± 0.10 ppm yr^{-1} in 2002 to 2.27 ± 0.03 ppm yr^{-1} in 2010 and

410 2.74 ± 0.10 ppm yr^{-1} in 2018. These values agree relatively well with the globally averaged values as measured by the NOAA's Global Monitoring Laboratory: 1.86 ± 0.20 ppm yr^{-1} in 2002, 1.97 ± 0.14 ppm yr^{-1} in 2010, and 2.57 ± 0.19 ppm yr^{-1} in 2018 (https://gml.noaa.gov/ccgg/trends/global.html). The values from NOAA are calculated based on a 5-year average around the time marks 2002, 2010 and 2018. In all three periods, the values at Mace Head are also in agreement with those of Lutjewad (1.86 ± 0.06 in 2002, 2.24 ± 0.02 in 2010, and 2.63 ± 0.06 ppm yr^{-1} in 2018 for Mace

415 Head). When averaging the trends over the 20-year period, both stations show good agreement with each other and with the global average: 2.31 ± 0.07 ppm yr^{-1} for Lutjewad, 2.22 ± 0.04 ppm yr^{-1} for Mace Head, and 2.1 ± 0.3 ppm yr^{-1} for global.

$\delta(O_2/N_2)$ measurements at Lutjewad also show a clear trend that becomes increasingly more negative throughout the

420 20 years. The trends (reported here in per meg yr^{-1} with their 95% CI uncertainties) in 2002, 2010, and 2018 are -18.01

± 1.17 per meg yr^{-1}, -20.99 ± 0.29 per meg yr^{-1}, and -23.98 ± 1.17 per meg yr^{-1}, respectively. At Mace Head, we find an unexpected trend: while CO_2 's trend increases, that of $\delta(O_2/N_2)$ becomes less negative (-22.4 ± 1.3 per meg yr^{-1}, -21.2 ± 0.3 per meg yr^{-1}, and -20.0 ± 1.3 per meg yr^{-1} in 2002, 2010, and 2018, respectively), which is contrary to the expectations of an increasingly negative trend, based on increased fossil fuel consumption over the years, and also

425 different from the measurements at Lutjewad. The lower number of flask samples from Mace Head between 2017 and 2019 makes it difficult to accurately interpret the cause of this change in the trend, and it also affects the determination of a proper fit through the period, potentially leading to inaccuracies in the long-term trend. When averaged over the entire period, however, both stations show almost identical trends: -21.2 ± 0.8 per meg yr^{-1} for Lutjewad and -21.3 ± 0.9 per meg yr^{-1} for Mace Head.

430

The APO trend and seasonality can be determined either from fitting the APO values of the individual flasks themselves, or by combining the trend/seasonal parameters of the $\delta(O_2/N_2)$ and CO_2 fits. Both methods yield almost identical results. We present here the results from the first approach. Since APO is calculated from the combination of $\delta(O_2/N_2)$ and CO_2 measurements, it shows a combination of the patterns as illustrated in the two species. The APO trend (reported here also in per meg yr^{-1}) at Lutjewad does not differ significantly over time, varying from -9.4 ± 0.8 per meg yr^{-1} in 2002

435 to -9.31 ± 0.20 per meg yr^{-1} in 2010, and -9.3 ± 0.8 per meg yr^{-1} in 2018. In Mace Head, however, the same pattern as $\delta(O_2/N_2)$ is shown for APO: the trend gets significantly less negative throughout the period (-13.15 ± 1.20 per meg yr^{-1} in 2002, -9.5 ± 0.3 per meg yr^{-1} in 2010, and -5.83 ± 1.20 per meg yr^{-1} in 2018).

440 Measurements at Halley station show a similar trend as Lutjewad and Mace Head, where CO_2 increases over time while $\delta(O_2/N_2)$ decreases, with much less variability in $\delta(O_2/N_2)$ and CO_2 measurements, due to the absence of a terrestrial biosphere influence. The averaged CO_2 trend at Halley from 2014 to 2017 is 2.60 ± 0.20 ppm yr^{-1}, similar to the trends at Lutjewad and Mace Head in the same period (2.62 ± 0.08 ppm yr^{-1} and 2.53 ± 0.05 ppm yr^{-1}, respectively). On the other hand, $\delta(O_2/N_2)$ and APO trends at Halley are significantly smaller in size than those at Lutjewad and Mace Head.

445 The $\delta(O_2/N_2)$ trend at Halley over the 2014-2017 period is -15 ± 3 per meg yr^{-1} while at Lutjewad and Mace Head, the trends are -23.2 ± 0.9 per meg yr^{-1}and -20.3 ± 1.0 per meg yr^{-1}, respectively. For APO, the corresponding values are -1.4 ± 2.4 per meg yr^{-1}, -9.3 ± 0.6 per meg yr^{-1}, and -6.7 ± 0.9 per meg yr^{-1}.
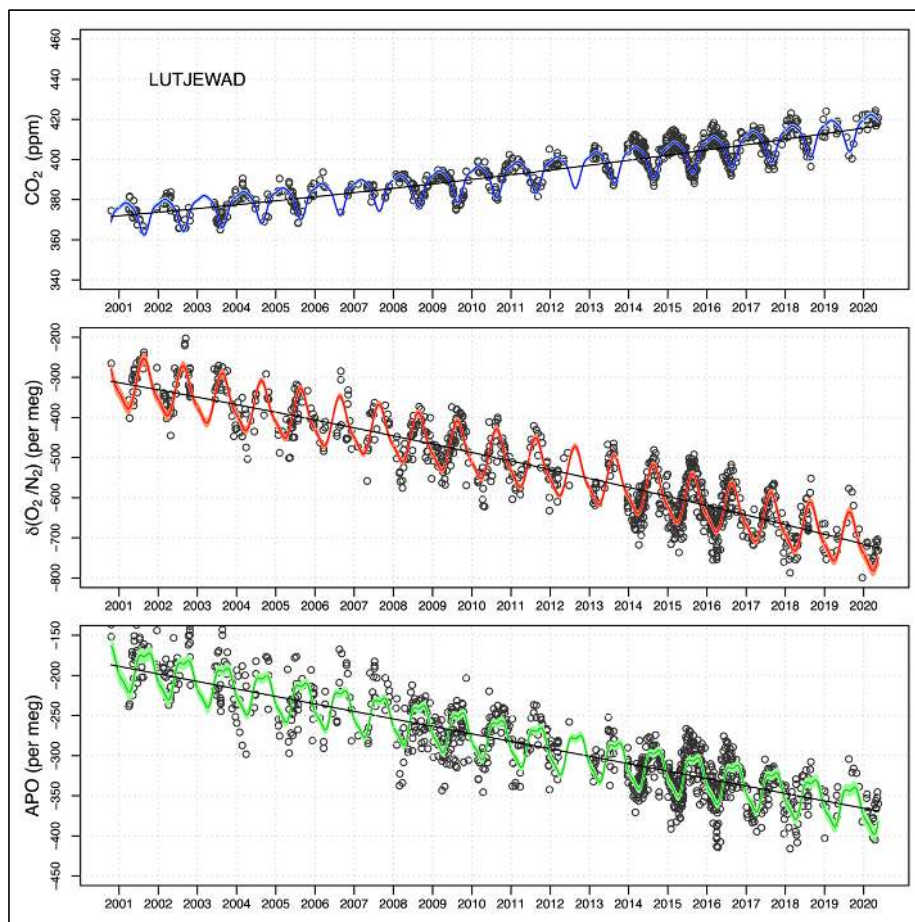
Figure 6: Flask record from Lutjewad station, showing CO_2, $\delta(O_2/N_2)$, and APO measurements from 2000 to 2020. The black
450 **points are the individual flask measurements, while the black lines are the long-term trend and the coloured lines indicate**
the trend with seasonal components derived from the combined quadratic and harmonic regression. The uncertainty ranges
(2-sigma) in the fits are indicated by lighter shades of the same colours. For comparability, the y-axes ranges are scaled to
represent the 5 per meg : 1 ppm ratio.

455
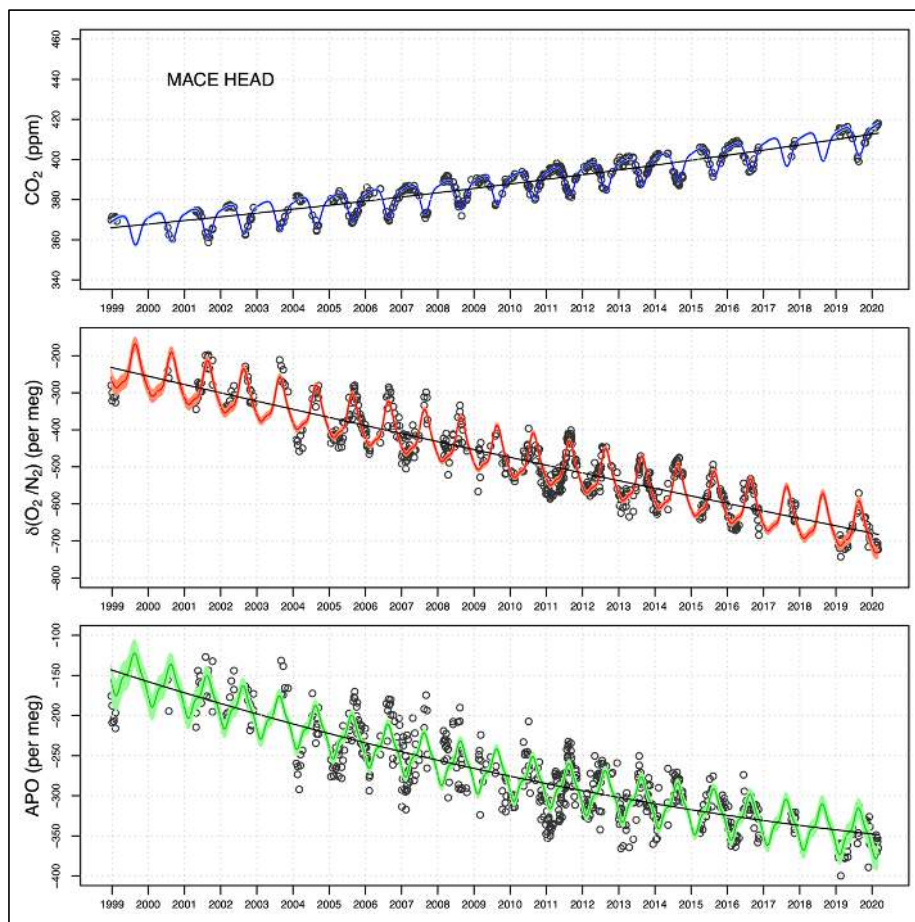
Figure 7: As for Fig. 6 but for Mace Head station.

460
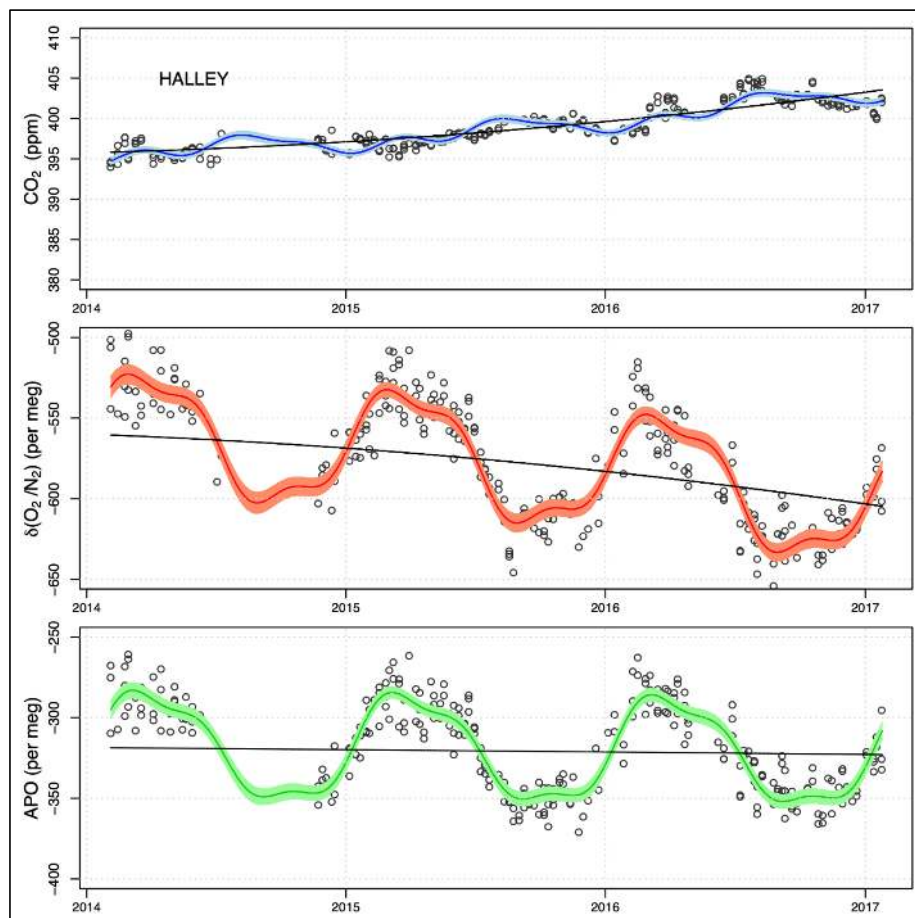
Figure 8: As for Fig. 6 and 7, but for Halley station and from 2014 to 2017.

4.2 Seasonal cycles

465   The seasonal cycles of CO_2, $\delta(O_2/N_2)$, and APO for all three stations are presented in Fig. 9. The seasonal components are extracted from the total fits (detrended) and presented as 1-year cycles. In general, the CO_2 seasonal cycles at Lutjewad and Mace Head are similar in size and shape, although the average seasonal amplitude is higher at Lutjewad (16.8 ± 0.5 ppm) than Mace Head (14.8 ± 0.3 ppm). The CO_2 seasonal cycle at Halley station, on the other hand, has a much smaller amplitude of 3.0 ± 0.3 ppm, as is generally the case for the ocean-dominated Southern Hemisphere due

470   to the absence of a terrestrial biosphere influence. Lutjewad and Mace Head show very similar, and significantly higher $\delta(O_2/N_2)$ seasonal amplitudes (131 ± 6 per meg and 130 ± 6 per meg, respectively) than that at Halley (76 ± 4 per meg), due to the influences of the terrestrial biosphere. In APO this influence is cancelled because APO is invariant to terrestrial biosphere processes, and the Halley amplitude is even somewhat higher than that of Lutjewad and Mace Head (65 ± 3 per meg compared to 54 ± 4 and 61 ± 5 per meg, respectively). All numerical seasonality parameters of the
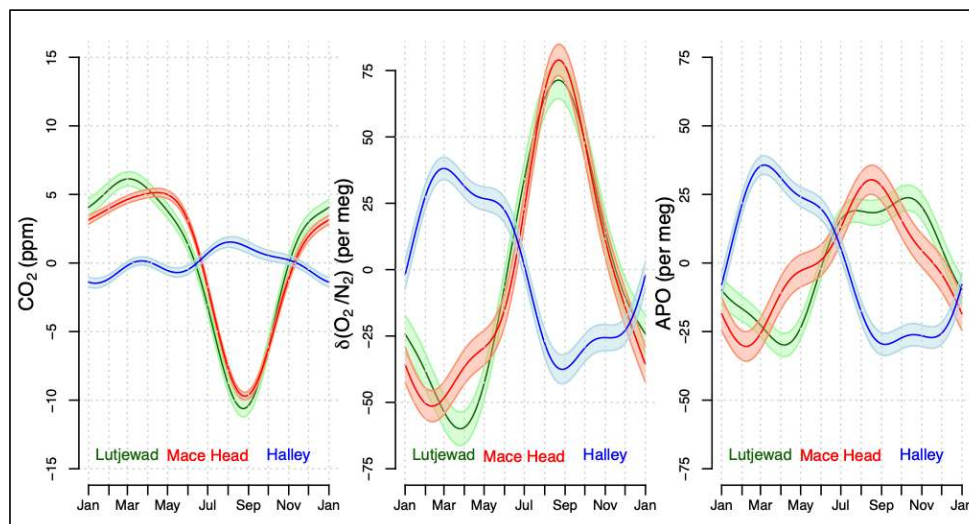
475   three stations are given in Table 4 below.

17

Figure 9: The detrended average seasonal cycles of CO₂ (left panel), δ(O₂/N₂) (middle panel), and APO (right panel) of stations Lutjewad (plotted in green), Mace Head (plotted in red), and Halley (plotted in blue). The uncertainty margins (2-sigma) in the fits have been indicated by lighter shades of the same colours.

480 **Table 4: Trend and seasonality fit parameters of the measurement records from all three stations, as presented in Fig. 6-8**

		Lutjewad (2002-2018)	Mace Head (2002-2018)	Halley (2014-2017)
CO_2	Seasonal amplitude (ppm)	16.8 ± 0.5	14.8 ± 0.3	3.0 ± 0.3
	Average trend (ppm/year)	2.31 ± 0.07	2.22 ± 0.04	2.60 ± 0.20
	Day of min. value	236 (Aug 24th) ± 13	238 (Aug 26th) ± 11	11 (Jan 11th) ± 12
	Day of max. value	62 (Mar 3rd) ± 26	105 (Apr 15th) ± 30	216 (Aug 4th) ± 14
$\delta(O_2/N_2)$	Seasonal amplitude (per meg)	131 ± 6	131 ± 6	76 ± 4
	Average trend (per meg/year)	-21.2 ± 0.8	-21.3 ± 0.9	-15 ± 3
	Day of min. value	85 (Mar 26th) ± 23	42 (Feb 11th) ± 33	239 (Aug 27th) ± 18
	Day of max. value	234 (Aug 22nd) ± 19	234 (Aug 22nd) ± 13	59 (Feb 28th) ± 21
APO	Seasonal amplitude (per meg)	54 ± 4	61 ± 5	65 ± 3
	Average trend (per meg/year)	-9.3 ± 0.5	-9.7 ± 0.9	-1.4 ± 2.4
	Day of min. value	96 (Apr 6th) ± 21	38 (Feb 7th) $+ 30$	250 (Sep 7th) ± 12
	Day of max. value	284 (Oct 11th) ± 29	229 (Aug 17th) ± 29	66 (Mar 7th) ± 17

5 Discussion

5.1 Measurements at Lutjewad, Mace Head, and Halley

Here, we discuss our measurement records in more detail. At first, the difference in the progression of trends in δ(O₂/N₂) and APO between Lutjewad and Mace Head (Fig. 6 and 7) suggests that there could be an issue with the flask sampling

485 procedure at Mace Head, such as the way the samples are dried. At Lutjewad, the sampling process has been under much closer controlled thanks to the vicinity of our laboratory enabling frequent visits, multiple tests and other measurements taken from the same sample lines. Furthermore, a comparison of the Lutjewad data with data from the nearby Weybourne coastal station in the UK (presented in Sect. 5.2) showed very good agreement. As both Lutjewad and Mace Head samples share the same measurement procedure, measurement and calibration issues cannot explain

490 their differences, so the differences must either be real, or related to the flask sampling procedure. It takes longer to transport the flasks from Mace Head to Groningen than from Lutjewad and thus contaminations of the samples through the valve caps might have occurred. For the samples from the Halley station, the transport time is even longer, but here, additional protective caps are used on the valve caps of the flasks to counteract permeation effects. We tested the preservation of the samples using the protective caps by sending flasks to Halley station that were pre-filled with air of
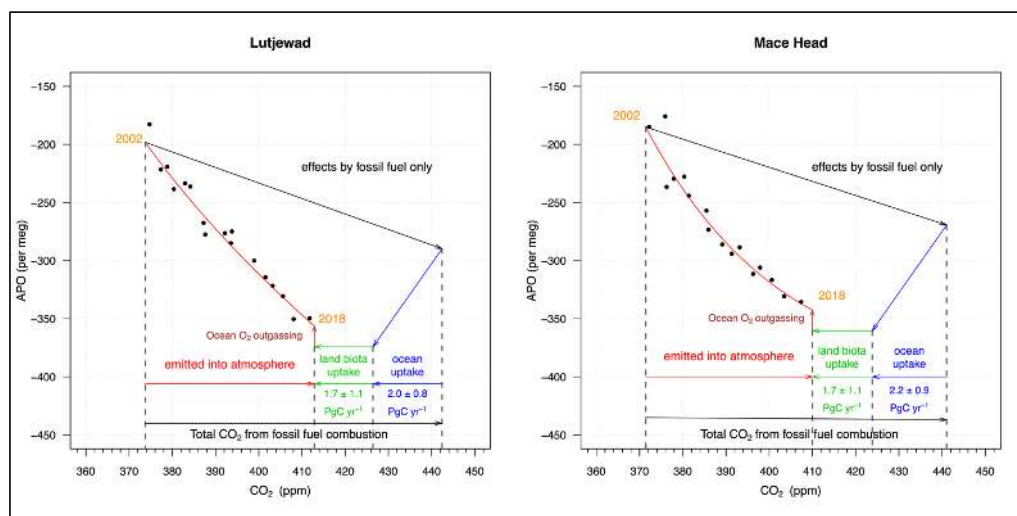
495 known composition, without actually using them. Back in Groningen, we could conclude the integrity of the samples by comparing the measurements before and after shipment, and we found no significant change in $\delta(O_2/N_2)$ after 26 to 51 months. Unfortunately, the protective caps were not applied to Mace Head samples. Still, it is hard to imagine how such permeation effects could cause a deviating long-term trend in the data given that the flasks were filled to ambient pressure. If anything, one would expect more scatter in the record. The same holds for sampling problems, such as

500 incomplete drying. To summarise, the trends at Lutjewad are as expected while those at Mace Head are not, so if there are no systematic sampling errors, the differences in $\delta(O_2/N_2)$ and APO in Mace Head compared to Lutjewad might be partially caused by the sparse and irregular sampling frequency at Mace Head. However, it is also worthwhile to consider effects that maybe caused by real environmental differences between the two stations. Two effects come to mind: the first is a difference in fossil fuel use (both in quantity and type), which would influence $\delta(O_2/N_2)$ and to a

505 lesser extent also APO. The average fossil fuel exchange ratio (ER) for the Netherlands, when accounting for all fossil fuel types, is 1.60 ± 0.02 for the 2000-2020 period, much higher than that for Mace Head (1.49, see van der Laan-Luijkx et al. (2010) and the CO_2 release and Oxygen uptake from Fossil Fuel Emission Estimate (COFFEE) database by (Steinbach et al., 2011)), and the global average value for all fossil fuel emissions (of 1.38), as also mentioned by Sirignano et al. (2010) and van der Laan-Luijkx et al. (2010). However, it is unlikely that this is the main explanation

510 of the difference between the two records. Firstly, because at Lutjewad, sampling was selective so as to avoid continental (and thus local fossil fuel) influences as much as possible, and second, because a difference in trends would need a gradual change in the ER. Data from Statistics Netherlands (CBS, 2021) show that the ER of the Netherlands has changed by no more than 0.02 over the period 2000-2020, too small to be of influence on the observed difference in the trends at Lutjewad and Mace Head.

515

A more likely cause for differences between Mace Head and Lutjewad are changes in North Atlantic oxygen ventilation (Keeling and Manning, 2014) to which the Mace Head observations are more sensitive. Such changes would influence $\delta(O_2/N_2)$ and APO, but not CO_2. This is consistent with the fact that the CO_2 trends of Mace Head and Lutjewad agree, whereas there are differences in $\delta(O_2/N_2)$ and APO. Changes in the oxygen inventory of the North Atlantic have been

520 reported by Stendardo and Gruber (2012) and Montes et al. (2016) and a relationship with the North Atlantic Oscillation (NAO) has been reported. Data obtained from the NOAA Climate Prediction Center (https://www.cpc.ncep.noaa.gov/data/teledoc/nao.shtml) show that the NAO exhibited gradual changes over the period 2000-2020, from a noisy, more or less balanced positive-negative pattern in the first decade, through to a negative phase in the years 2010-2011 towards gradually mostly positive values for the period 2013-2019.

525

When comparing the seasonal cycles of the three stations, we can see that while CO_2 and $\delta(O_2/N_2)$ seasonal amplitudes at Halley are significantly smaller than those at Lutjewad and Mace Head, the APO seasonal amplitude is slightly higher, agreeing with the model simulation by Tohjima et al. (2012) that the APO seasonal variations in the Southern Hemispheric ocean are larger than those in the Northern Hemisphere due to larger air-sea O_2 exchange. As mentioned

530 in Sect. 2, APO values also contain a small influence from fossil fuels, however, by selecting for flasks based on the background conditions, we eliminate as much as possible this influence, especially for the Lutjewad record. As such, our APO values from these three stations represent mostly ocean influences.

To conclude the comparison between Lutjewad and Mace Head, we calculated the partitioning of CO_2 uptake by the

535 terrestrial biosphere and the ocean from the observations at the two stations, using the measurements of CO_2 and APO concentrations at Lutjewad and Mace Head from 2002 to 2018, via the method described by Keeling and Manning (2014). This partitioning is illustrated in Fig. 10.

Figure 10: Vector diagrams presenting the calculation of the global land biotic and oceanic carbon sinks for the 2002-2018
540 **period. The black points are the annual averages of the measured APO and CO₂ values at Lutjewad (left panel) and Mace Head (right panel). The black arrowed line represents the changes in the atmospheric APO and CO₂ values that would have occurred if all CO₂ emitted from fossil fuel combustion remained in the atmosphere. The ocean uptake is presented by blue arrows and its slope is fixed to the APO/CO₂ molar ratio of 1.1 (that represents the removal of the biosphere signal in the definition of APO). The land biota uptake (green) is a horizontal line, as APO does not include a biosphere signal. The ocean**
545 **O₂ outgassing effect is plotted in brown.**

The black points are the annual averages of the de-seasonalised measurements of APO and CO_2 concentrations at Lutjewad and Mace Head for the period 2002-2018, and clearly show the unexpected trend in APO for Mace Head, as discussed above. For calculating the partitioning of fossil fuel CO_2, we use, from Keeling and Manning (2014), equations (2) to (10), and the ocean O_2 outgassing component (Z) of $0.44 \pm 0.45 \cdot 10^{14}$ mol yr^{-1} (equivalent to an effect

550 on the carbon sinks of 0.46 ± 0.48 PgC yr^{-1}). Furthermore, we use the total fossil fuel component for the years 2002-2018 of 8.6 ± 0.6 PgC yr^{-1} as derived from the Global Carbon Budget 2020 by Friedlingstein et al. (2020), and the ER for globally averaged fossil fuel combustion of 1.38 ± 0.03 from Keeling and Manning (2014). From the Lutjewad record, the global land biotic sink (B) is 1.7 ± 1.1 PgC yr^{-1}, the oceanic sink (O) is 2.0 ± 0.8 PgC yr^{-1}, and the CO_2 remaining in the atmosphere (A) amounts to 4.91 ± 0.15 PgC yr^{-1}. The values calculated from Mace Head record are

555 very similar to those from Lutjewad: at Mace Head, B is 1.7 ± 1.1 PgC yr^{-1}, O is 2.2 ± 0.9 PgC yr^{-1} and A is 4.72 ± 0.09 PgC yr^{-1}. For both stations, the values for the B and O components agree well with those reported by Friedlingstein et al. (2020): 1.7 ± 1.6 GtC yr^{-1} for B (including emissions from land-use changes) and 2.3 ± 0.8 GtC yr^{-1} for O. The values for A as measured at both Lutjewad and Mace Head are slightly higher than the reported average value of 4.63 ± 0.03 PgC yr^{-1} for the 2002-2018 period.

560

The challenges in making O_2 measurements have presented themselves clearly in this work: the sensitivity of the mass spectrometer that require intensive calibration; the quality maintenance of the internal calibration scale to make sure that our measurements can be reported with sufficient quality on the international scale; and the unexpected patterns (especially in APO for Mace Head) that could not be fully explained, partly due to the lack of consistent sampling

565 frequency before 2004 (for both stations), during 2012 (for Lutjewad) and between 2017 and 2019 (for Mace Head). The trend and seasonality fitting procedure are also of great importance, as these are also highly sensitive to irregular sampling frequency and biases in the timing in which the majority of the samples is collected. Nevertheless, our flask measurement records of Lutjewad, Mace Head, and Halley have proven to be informative and valuable in evaluating APO, and with future technical improvement (especially regarding the sampling frequency and the quality maintenance

570   of our internal scale), they will be extended further. In the near future, in addition to more regular sampling frequency
      at Lutjewad and Mace Head, we aim to improve the frequency at which we perform the measurements on the SIO
      primary standard cylinders, and also to purchase new primary standard cylinders from them, to produce higher precision
      conversion to the SIO scale. We also aim to employ more WTs as the current ones are either running out or experiencing
      considerable noise (see WT 4845 in Fig. 3). More protective measures to the flasks, such as using additional caps or
575   switching to another type of valve, will also be considered, to reduce the risks of potential leakages, permeations, and
      contaminations during storage and transportation.

5.2 Comparison with other long-term records

      In Table 5, we compare the seasonal amplitudes of our CO_2, $\delta(O_2/N_2)$, and APO measurements with those of some
      other stations worldwide. As can be seen, the measurements for all three species at Lutjewad and Mace Head agree well
580   with the measurements conducted at other Northern Hemisphere stations Weybourne (UK), Sendai (Japan), and Ny
      Ålesund (Norway). In the Southern Hemisphere, our $\delta(O_2/N_2)$ and APO measurements for Halley station show an
      excellent agreement with those at the Syowa station. On the other hand, our CO_2 measurements exhibit a much larger
      and noisier seasonal amplitude, which is most likely caused by small leaks during sampling (the details of which are
      given at the end of this section). Nonetheless, the general concurrence with these stations helps to consolidate the quality
585   of our measurements.

Table 5: Comparison of the seasonal amplitudes of CO_2, $\delta(O_2/N_2)$, and APO at various locations in the world

Station	Time period	Latitude	CO_2 (ppm)	$\delta(O_2/N_2)$ (per meg)	APO (per meg)	Reference
Ny Ålesund, Spitsbergen	2001-2010	79°N	15.2 ± 0.4	129 ± 4	52 ± 3	Ishidoya et al. (2012b)
Weybourne, UK	2008-2015	53°N	15.2 ± 1.1	130 ± 8	51 ± 6	(Barningham, 2018)
Lutjewad, the Netherlands	2002-2018	53°N	16.8 ± 0.5	131 ± 6	54 ± 4	This paper
Mace Head, Ireland	2002-2018	53°N	14.8 ± 0.3	130 ± 6	61 ± 5	This paper
Sendai, Japan	1999-2012	38°N	13.9 ± 2.5	128 ± 22	52 ± 10	Ishidoya et al. (2012a)
Syowa station, Antarctica	2001-2010	69°S	1.1 ± 0.04	70 ± 4	64 ± 4	Ishidoya et al. (2012b)
Halley station, Antarctica	2014-2017	75°S	3.0 ± 0.3*	76 ± 4	65 ± 3	This paper

*The CO_2 seasonal amplitude at Halley is most likely incorrect, details are given at the end of this section.

      Additionally, we compare our long-term measurement record with an extended record of Weybourne station (Fig. 11),
590   the first part of which has been published by Pickers (2016) and Barningham (2018). Because of differences between
      continuous and flask sampling frequency, there are large differences between the two records, obviously in the amount
      of data points, but also in the height of the peaks and troughs during the diurnal cycle, and also the temporal length of
      the peaks and troughs. This is mostly because our flask samples at Lutjewad are collected during background conditions
      (and further selected for even more strict conditions during analyses) and are sometimes irregular in time, whereas the
595   measurements at Weybourne are continuous (and therefore also represent local events). However, when considering
      background conditions at Weybourne (the lower limits of CO_2 and upper limits of $\delta(O_2/N_2)$), there is good agreement
      with the Lutjewad record.
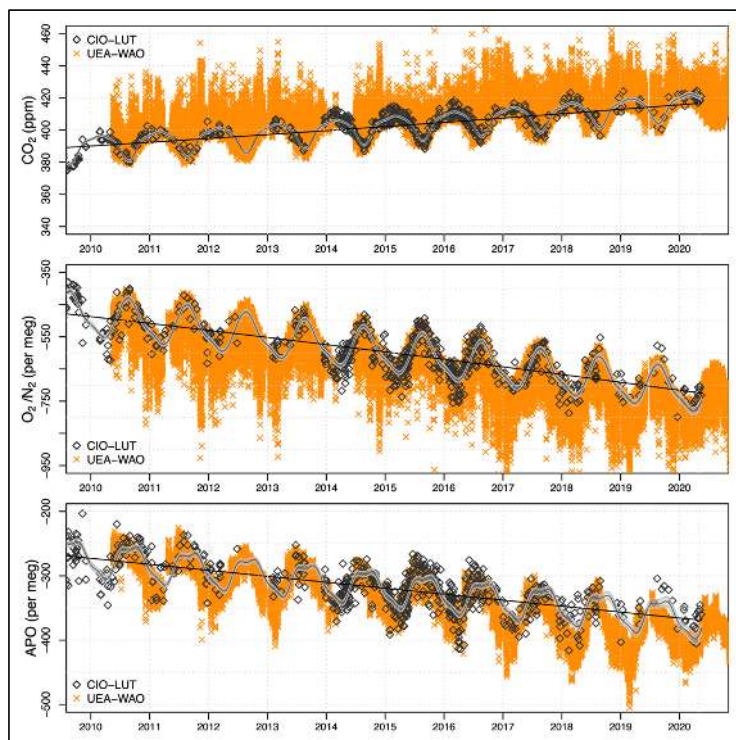
Figure 11: Measurements of CO₂, δ(O₂/N₂), and APO at Lutjewad (black diamonds) and Weybourne (orange crosses) from
600 **2010 to 2020. The black line and curve are the trend and the combined fit for Lutjewad, respectively. The grey shadings are**
the 95% CI associated with the total fit.

For Halley, we compare our CO_2, $\delta(O_2/N_2)$, and APO measurements with those conducted by UEA (Fig. 12)
(Barningham, 2018). APO measurements between our laboratory and UEA show good agreement, while CO_2
measurements show unexpected discrepancies in the first half of 2016. $\delta(O_2/N_2)$ measurements also show a slight
605   disagreement, but it is less visible due to a large seasonal cycle and higher scatter. Because APO agrees well, we
conclude that the CO_2 and $\delta(O_2/N_2)$ anomalies were most likely caused by a small inwards leak when the flask samples
were collected at the station. Laboratory air with higher CO_2 mole fractions and lower $\delta(O_2/N_2)$ ratios due to human
breathing, probably leaked in. An additional indication pointing to this is that the CH_4 and CO mole fractions from the
same flasks agree very well with long-term flask measurements made at Halley by NOAA (NOAA, 2021) (not shown
610   here). Such leaks do not influence APO, as the ER from human breathing is close to the value of 1.1 used for the
exclusion of the biosphere signal in APO. To better check how much these anomalies would have affected our
measurements, we use the long-term flask measurements made at Halley from the NOAA website
(https://gml.noaa.gov/dv/iadv/graph.php?code=HBA&program=ccgg&type=ts.), since the UEA's measurement period
is too short to make a reliable comparison. For CO_2, we perform the trend and seasonality fitting procedure, the same
615   as for our own measurements. For APO, since there is no available information on O_2, we combine the NOAA's CO_2
measurements with our own $\delta(O_2/N_2)$ measurements to calculate APO, then proceeded with the fitting of the trend and
seasonality. Plotted in blue are the results using the NOAA's CO_2 measurements. Leakages would lead to higher CO_2
mole fraction and lower $\delta(O_2/N_2)$ ratio than the background sample, but APO would largely cancel them. We now
combine the background CO_2 measurements from NOAA and the $\delta(O_2/N_2)$ values from our (supposedly contaminated)
620   flask measurements, and indeed a clear bias in the APO can be seen coinciding with the CO_2 anomalies. This confirms
the presence of some contamination in a number of our flasks, especially during March-June 2016 and in early 2014.
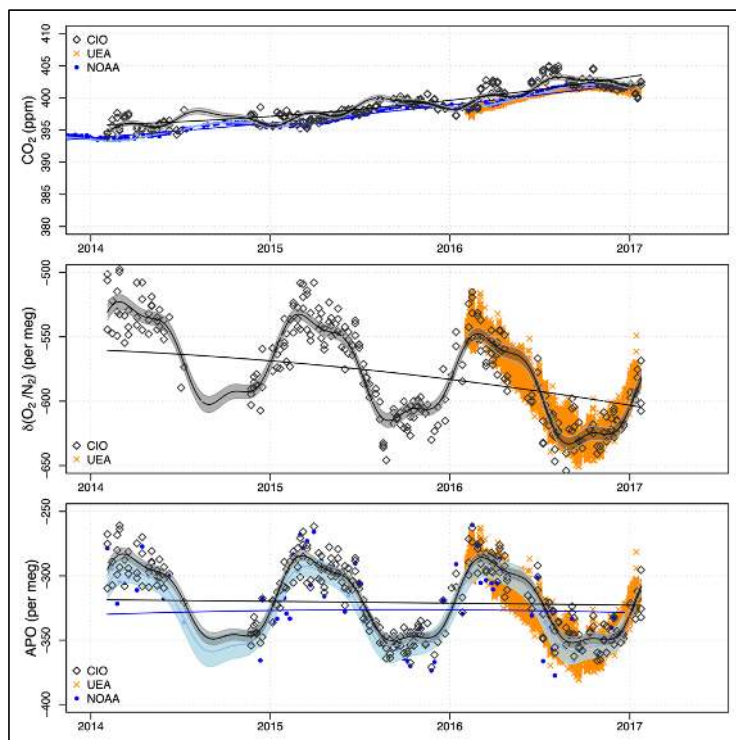
Figure 12: Measurements of CO_2, $\delta(O_2/N_2)$, and APO at Halley conducted by CIO (black diamonds) from 2014 to 2017, and continuous measurements conducted by UEA (orange crosses) in 2016. The black lines and curves are the trends and the combined fit for measurements by CIO, respectively. The grey shaded area is the 95% CI associated with the total fit. The blue points are the in-situ continuous measurements at Halley, taken by NOAA. The blue lines and curves are the trends and the combined fits for the continuous measurements, with the lighter blue shaded area the 95% CI associated with the total fit. From the combination of all data we conclude that our CO_2 measurements must have been contaminated with inside air (human breathing).

6 Conclusion

We have presented 20-year flask measurement records for $\delta(O_2/N_2)$, CO_2 and APO from Lutjewad and Mace Head, along with 3-year records from Halley. We also presented results of the calibration procedures of our instruments. Due to the sensitive nature of oxygen measurements, we conducted an extensive and intensive calibration procedures, which demonstrated a long-term standard deviation for $\delta(O_2/N_2)$ of 13.5 per meg based on our own internal cylinders. Measurements of the global primary standard cylinders (from SIO) and inter-comparison cylinders (from the Cucumber and GOLLUM programmes) consolidate the stability, quality, and comparability of our calibration procedure, although there are some indications that our calibration scale might not be entirely stable over the past 20 years. However, the results from those various programmes are not consistent, and therefore inconclusive. The long-term records from Lutjewad and Mace Head provided useful information on the two-decadal trends and seasonality of CO_2, $\delta(O_2/N_2)$, and APO, showing good agreements with other stations around the world, especially the Weybourne Atmospheric Observatory in the UK. We found long term trends during the period 2002-2018 of 2.31 ± 0.07 ppm yr^{-1} for CO_2 and -21.2 ± 0.8 per meg yr^{-1} for $\delta(O_2/N_2)$ at Lutjewad, and 2.22 ± 0.04 ppm yr^{-1} for CO_2 and -21.3 ± 0.9 per meg yr^{-1} for $\delta(O_2/N_2)$ at Mace Head. The notable differences in the year-to-year progression of $\delta(O_2/N_2)$ and APO trends between Lutjewad and Mace Head might in part be caused by the sparse sampling frequency at Mace Head, but also may be indications of real influences from the various types of fossil fuel used, or from changes in ocean O_2 ventilation. Using the measurements at Lutjewad for 2002-2018, the partitioning of atmospheric CO_2 sinks into the global terrestrial

biosphere and the oceans are 1.7 ± 1.1 PgC yr^1 and 2.0 ± 0.8 PgC yr^{-1}, respectively, and when calculated using the Mace Head record, these are 1.7 ± 1.1 PgC yr^{-1} and 2.2 ± 0.9 PgC yr^{-1}, respectively. These values agree well with the numbers reported in the most recent Global Carbon Budget. The Halley record shows that the APO seasonal variations in the

650 Southern Ocean are slightly larger than those in the Northern Hemisphere due to larger air-sea O_2 exchange there, and illustrats clearly the influences of oceanic processes on the variations in APO and atmospheric O_2. With better maintenance of our internal scale, more regular sampling frequency, and better quality-control of the sampling process, the reliability of our future flask measurements will be improved.

Data availability

655 The accompanying database comprises three csv files. The files contain the information on the CO_2, $\delta(O_2/N_2)$, and APO measurements (measured values and associated uncertainties) of the three stations, and are named after the corresponding station and the measured parameter (9 files in total).

All files are published by the ICOS Carbon Portal, and are available at https://doi.org/10.18160/qq7d-t060 (Nguyen et
660 al., 2021).

The additional data presented in this paper are available upon request.

Author contributions

LNTN, HAJM, and ITL conducted the data analyses, produced all figures and tables, and wrote the manuscript. ITL
665 and HAJM designed the methodology and framework for the calibration procedure of the DI-IRMS. BAMK conducted the technical work and prepared the flask samples at Lutjewad station, and carried out the CO_2 and $\delta(O_2/N_2)$ measurements from flasks collected at all three stations. HAS calibrated the CO_2 data at CIO. AEJ, NB, and TB performed the measurements at Halley station, prepared the flask samples, produced the data for comparison. PAP and ACM provided the data from Weybourne station. All co-authors contributed to the writing of the manuscript.

670 **Competing interests**

The authors declare that they have no conflict of interest.

690   **References**

Aoki, N., Ishidoya, S., Tohjima, Y., Morimoto, S., Keeling, R. F., Cox, A., Takebayashi, S., and Murayama, S.: Inter-
comparison of O_2/N_2 Ratio Scales Among AIST, NIES, TU, and SIO Based on Round-Robin Using Gravimetric
Standard Mixtures, Atmos. Meas. Tech. Discuss. [preprint], 2021, 1-26, 10.5194/amt-2020-481, 2021.

Barningham, T.: Detection and Attribution of Carbon Cycle Processes from Atmospheric O_2 and CO_2 Measurements
695   at Halley Research Station, Antarctica and Weybourne Atmospheric Observatory, U.K., PhD Thesis, School of
Environmental Sciences, University of East Anglia, Norwich, United Kingdom, 2018.

Battle, M., Fletcher, S. M., Bender, M. L., Keeling, R. F., Manning, A. C., Gruber, N., Tans, P. P., Hendricks, M. B.,
Ho, D. T., Simonds, C., Mika, R., and Paplawsky, B.: Atmospheric potential oxygen: New observations and their
implications for some atmospheric and oceanic models, Global Biogeochemical Cycles, 20, n/a-n/a,
700   10.1029/2005gb002534, 2006.

Bender, M. L., Ellis, T., Tans, P. P., Francey, R., and Lowe, D.: Variability in the O_2/N_2 ratio of southern hemisphere
air, 1991–1994: Implications for the carbon cycle, Global Biogeochemical Cycles, 10, 9 - 21, 1996.

Bender, M. L., Tans, P. P., Ellis, T., Orchardo, J., and Habfast, K.: A high precision isotope ratio mass spectrometry
method for measuring the O_2/N_2 ratio of air, Geochimica et Cosmochimica Acta,, 58, 4751 - 4758, 1994.

705   Blaine, T. W., Keeling, R. F., and Paplawsky, W. J.: An improved inlet for precisely measuring the atmospheric
Ar/N_2 ratio, Atmos. Chem. Phys., 6, 1181-1184, 10.5194/acp-6-1181-2006, 2006.

Bousquet, P., Gaudry, A., Ciais, P., Kazan, P., Monfray, P., Simmonds, P. G., Jennings, S. G., and O'Connor, T. C.:
Atmospheric CO_2 Concentration Variations Recorded at Mace Head, Ireland, From 1992 to 1994, Phys. Chem. Earth,
21, 477 - 481, 1996.

710   Halley VI Research Station: https://www.bas.ac.uk/polar-operations/sites-and-facilities/facility/halley/, last access:
02/04/2021.

The Netherlands in figures: https://opendata.cbs.nl/statline/#/CBS/en/, last access: 22/04/2021.

Chen, H., Winderlich, J., Gerbig, C., Hoefer, A., Rella, C. W., Crosson, E. R., Van Pelt, A. D., Steinbach, J., Kolle,
O., Beck, V., Daube, B. C., Gottlieb, E. W., Chow, V. Y., Santoni, G. W., and Wofsy, S. C.: High-accuracy
715   continuous airborne measurements of greenhouse gases (CO_2 and CH_4) using the cavity ring-down spectroscopy
(CRDS) technique, 3, 375 - 386, 2010.

Ciais, P., Sabine, C., Bala, G., Bopp, L., Brovkin, V., Canadell, J., Chhabra, A., DeFries, R., Galloway, J., Heimann, M., C., J., C., L. Q., Myneni, R. B., Piao, S., and Thornton, P.: Carbon and Other Biogeochemical Cycles, in: Climate Change 2013: The Physical Science Basis. Contribution of Working Group I to the Fifth Assessment Report of the Intergovernmental Panel on Climate Change edited by: Stocker, T. F., D. Qin, G.-K. Plattner, M. Tignor, S.K. Allen, J. Boschung, A. Nauels, Y. Xia, V. Bex and P.M. Midgley, Cambridge University Press, Cambridge, United Kingdom and New York, NY, USA, 2013.

Conway, T. J., Tans, P. P., and Waterman, L. S.: Atmospheric CO_2 records from sites in the NOAA/CMDL air sampling network, in: Trends '93: a compendium of data on global change, ORNL/CDIAC-65, Oak Ridge National Laboratory, USA, 1994.

Derwent, R. G., Ryall, D. B., Manning, A. J., Simmonds, P. G., O'Doherty, S., Biraud, S., Ciais, P., Ramonet, M., and Jennings, S. G.: Continuous observations of carbon dioxide at Mace Head, Ireland from 1995 to 1999 and its net European ecosystem exchange, Atmospheric Environment, 36, 2799 - 2807, 2002.

Friedlingstein, P., O'Sullivan, M., Jones, M. W., Andrew, R. M., Hauck, J., Olsen, A., Peters, G. P., Peters, W., Pongratz, J., Sitch, S., Le Quéré, C., Canadell, J. G., Ciais, P., Jackson, R. B., Alin, S., Aragão, L. E. O. C., Arneth, A., Arora, V., Bates, N. R., Becker, M., Benoit-Cattin, A., Bittig, H. C., Bopp, L., Bultan, S., Chandra, N., Chevallier, F., Chini, L. P., Evans, W., Florentie, L., Forster, P. M., Gasser, T., Gehlen, M., Gilfillan, D., Gkritzalis, T., Gregor, L., Gruber, N., Harris, I., Hartung, K., Haverd, V., Houghton, R. A., Ilyina, T., Jain, A. K., Joetzjer, E., Kadono, K., Kato, E., Kitidis, V., Korsbakken, J. I., Landschützer, P., Lefèvre, N., Lenton, A., Lienert, S., Liu, Z., Lombardozzi, D., Marland, G., Metzl, N., Munro, D. R., Nabel, J. E. M. S., Nakaoka, S.-I., Niwa, Y., O'Brien, K., Ono, T., Palmer, P. I., Pierrot, D., Poulter, B., Resplandy, L., Robertson, E., Rödenbeck, C., Schwinger, J., Séférian, R., Skjelvan, I., Smith, A. J. P., Sutton, A. J., Tanhua, T., Tans, P. P., Tian, H., Tilbrook, B., van der Werf, G., Vuichard, N., Walker, A. P., Wanninkhof, R., Watson, A. J., Willis, D., Wiltshire, A. J., Yuan, W., Yue, X., and Zaehle, S.: Global Carbon Budget 2020, Earth System Science Data, 12, 3269-3340, 10.5194/essd-12-3269-2020, 2020.

GOLLUM comparison: Manning, A. C., Keeling, R. F., Etchells, A. J., Hewitt, M., Bender, M. L., Bracchi, K., Brailsford, G. W., Brand, W. A., Cassar, N., Cox, A. C., Leuenberger, M., Meijer, H. A. J., Morimoto, S., Nakazawa, T., Neubert, R. E. M., Paplawsky, W. J., Richter, J. M., Stephens, B. B., Tohjima, Y., van der Laan, S., van der Laan-Luijkx, I. T., Watt, A., and Wilson, P. A.: The "GOLLUM" O2 intercomparison programme: Latest results and next step, Second APO Workshop La Jolla, California, U.S.A., https://gollum.uea.ac.uk/.

Gruber, N., Gloor, M., Fan, S.-M., and Sarmiento, J. L.: Air-sea flux of oxygen estimated from bulk data: Implications For the marine and atmospheric oxygen cycles, Global Biogeochemical Cycles, 15, 783-803, 10.1029/2000gb001302, 2001.

Hall, B. D., Crotwell, A. M., Kitzis, D. R., Meffor, T., Miller, B. R., Schibig, M. F., and Tans, P. P.: Revision of the WMO/GAW CO_2 Calibration Scale, Atmos. Meas. Tech. Discuss. [preprint], https://doi.org/10.5194/amt-2020-408, 2020.

Ishidoya, S., Aoki, S., Goto, D., Nakazawa, T., Taguchi, S., and Patra, P.: Time and space variations of the O_2/N_2 ratio in the troposphere over Japan and estimation of the global CO_2 budget for the period 2000–2010, Tellus B: Chemical and Physical Meteorology, 64, 10.3402/tellusb.v64i0.18964, 2012a.

Ishidoya, S., Morimoto, S., Aoki, S., Taguchi, S., Goto, D., Murayama, S., and Nakazawa, T.: Oceanic and terrestrial

755   biospheric CO_2 uptake estimated from atmospheric potential oxygen observed at Ny-Ålesund, Svalbard, and Syowa, Antarctica, Tellus B: Chemical and Physical Meteorology, 64, 10.3402/tellusb.v64i0.18924, 2012b.

Jennings, S. G., McGovern, F. M., and Cooke, W. F.: Carbon Mass Concentration Measurements at Mace Head, on the West Coast of Ireland, Atmospheric Environment, 27A, 1229 - 1239, 1993.

Jones, A. E., Wolff, E. W., Salmon, R. A., Bauguitte, S. J. B., Roscoe, H. K., Anderson, P. S., Ames, D., Clemitshaw,

760   K. C., Fleming, Z. L., Bloss, W. J., Heard, D. E., Lee, J. D., Read, K. A., Hamer, P., Shallcross, D. E., Jackson, A. V., Walker, S. L., Lewis, A. C., Mills, G. P., Plane, J. M. C., Saiz-Lopez, A., Sturges, W. T., and Worton, D. R.: Chemistry of the Antarctic Boundary Layer and the Interface with Snow: an overview of the CHABLIS campaign, Atmos. Chem. Phys., 8, 3789-3803, 10.5194/acp-8-3789-2008, 2008.

Keeling, R. F.: Development of an Interferometric Oxygen Analyzer for Precise Measurement of the Atmospheric O_2

765   Mole Fraction, PhD Thesis, Division of Applied Sciences, Harvard University, Cambridge, Massachusetts, 1988.

Keeling, R. F. and Manning, A. C.: 5.15 - Studies of Recent Changes in Atmospheric O_2 Content, in: Treatise on Geochemistry, 2nd ed., edited by: Holland, H. D., and Turekian, K. K., 10.1016/B978-0-08-095975-7.00420-4, 2014.

Keeling, R. F. and Shertz, S. R.: Seasonal and interannual variations in atmospheric oxygen and implications for the global carbon cycle, Nature, 358, 723 - 727, https://doi.org/10.1038/358723a0, 1992.

770   Keeling, R. F., Manning, A. C., McEvoy, E. M., and Shertz, S. R.: Methods for measuring changes in atmospheric O_2 concentration and their application in southern hemisphere air, Journal of Geophysical Research: Atmospheres, 103, 3381-3397, 10.1029/97jd02537, 1998.

Keeling, R. F., Blaine, T., Paplawsky, B., Katz, L., Atwood, C., and Brockwell, T.: Measurement of changes in atmospheric Ar/N_2 ratio using a rapid-switching, single-capillary mass spectrometer system, Tellus B: Chemical and

775   Physical Meteorology, 56, 322-338, 10.3402/tellusb.v56i4.16453, 2004.

Manning, A. C. and Keeling, R. F.: Global oceanic and land biotic carbon sinks from the Scripps atmospheric oxygen flask sampling network, Tellus, 58B, 95 - 116, 2006.

Manning, A. C., Keeling, R. F., and Severinghaus, J.: Precise atmospheric oxygen measurements with a paramagnetic oxygen analyzer, Global Biogeochemical Cycles, 13, 1107 - 1115, 1999.

780   Montes, E., Muller-Karger, F. E., Cianca, A., Lomas, M. W., Lorenzoni, L., and Habtes, S.: Decadal variability in the oxygen inventory of North Atlantic subtropical underwater captured by sustained, long-term oceanographic time series observations, Global Biogeochemical Cycles, 30, 460-478, https://doi.org/10.1002/2015GB005183, 2016.

Neubert, R. E. M., Spijkervet, L. L., Schut, J. K., Been, H. A., and Meijer, H. A. J.: A Computer-Controlled Continuous Air Drying and Flask Sampling System, Journal of Atmospheric and Oceanic Technology, 21, 2004.

785   Nguyen, L. N. T., Meijer, H. A. J., van Leeuwen, C., Kers, B. A. M., Scheeren, B. A., Jones, A. E., Brough, N., Barningham, T., Pickers, P. A., Manning, A. C., and Luijkx, I. T.: Supplement data of the Two decades of flask observations of atmospheric $\delta O_2/N_2$, CO_2, and APO at stations Lutjewad (the Netherlands) and Mace Head (Ireland) plus 3 years from Halley station (Antarctica), ICOS-ERIC Carbon Portal, https://doi.org/10.18160/qq7d-t060, 2021.

Carbon Cycle Gasses Halley Station, Antarctica, United Kingdom:

790   https://www.esrl.noaa.gov/gmd/dv/iadv/graph.php?code=HBA&program=ccgg&type=ts, last access: 02/04/2021.

Pickers, P. A.: New applications of continuous atmospheric O_2 measurements: meridional transects across the
Atlantic Ocean, and improved quantification of fossil fuel-derived CO_2, PhD Thesis, School of Environmental
Sciences, University of East Anglia, Norwich, United Kingdom, 2016.

Pickers, P. A., Manning, A. C., Sturges, W. T., Le Quéré, C., Mikaloff Fletcher, S. E., Wilson, P. A., and Etchells, A.

795   J.: In situ measurements of atmospheric O_2 and CO_2 reveal an unexpected O_2 signal over the tropical Atlantic Ocean,
Global Biogeochemical Cycles, 31, 1289-1305, 10.1002/2017gb005631, 2017.

Rousseeuw, P. J. and Verboven, S.: Robust estimation in very small samples, Computational Statistics & Data
Analysis, 40, 741-758, 2002.

Severinghaus, J. P.: Studies of the terrestrial O_2 and carbon cycles in sand dune gases and in biosphere 2, PhD Thesis,

800   United States, https://doi.org/10.2172/477735, 1995.

Sirignano, C., Neubert, R. E. M., Rödenbeck, C., and Meijer, H. A. J.: Atmospheric oxygen and carbon dioxide
observations from two European coastal stations 2000-2005: continental influence, trend changes and APO
climatology, Atmos. Chem. Phys., 10, 1599-1615, https://doi.org/10.5194/acp-10-1599-2010, 2010.

Steinbach, J., Gerbig, C., Rödenbeck, C., Karstens, U., Minejima, C., and Mukai, H.: The CO_2 release and Oxygen

805   uptake from Fossil Fuel Emission Estimate (COFFEE) dataset: effects from varying oxidative ratios, Atmos. Chem.
Phys., 11, 6855-6870, doi:10.5194/acp-11-6855-2011, 2011.

Stendardo, I. and Gruber, N.: Oxygen trends over five decades in the North Atlantic, Journal of Geophysical
Research: Oceans, 117, https://doi.org/10.1029/2012JC007909, 2012.

Stephens, B. B., Keeling, R. F., and Paplawsky, W. J.: Shipboard measurements of atmospheric oxygen using a

810   vacuum-ultraviolet absorption technique, Tellus B: Chemical and Physical Meteorology, 55, 857-878,
10.3402/tellusb.v55i4.16386, 2003.

Stephens, B. B., Bakwin, P. S., Tans, P. P., Teclaw, R. M., and Baumann, D. D.: Application of a Differential Fuel-
Cell Analyzer for Measuring Atmospheric Oxygen Variations, Journal of Atmospheric and Oceanic Technology, 24,
82-94, 10.1175/jtech1959.1, 2007.

815   Stephens, B. B., Keeling, R. F., Heimann, M., Six, K. D., Murnane, R., and Caldeira, K.: Testing global ocean carbon
cycle models using measurements of atmospheric O_2 and CO_2 concentration, Global Biogeochemical Cycles, 12, 213-
230, 10.1029/97gb03500, 1998.

Stephens, B. B., Morgan, E. J., Bent, J. D., Keeling, R. F., Watt, A. S., Shertz, S. R., and Daube, B. C.: Airborne
measurements of oxygen concentration from the surface to the lower stratosphere and pole to pole, Atmos. Meas.

820   Tech., 14, 2543-2574, 10.5194/amt-14-2543-2021, 2021.

Sturm, P., Leuenberger, M., Sirignano, C., Neubert, R. E. M., Meijer, H. A. J., Langenfelds, R., Brand, W. A., and
Tohjima, Y.: Permeation of atmospheric gases through polymer O-rings used in flasks for air sampling, Journal of
Geophysical Research: Atmospheres, 109, n/a-n/a, 10.1029/2003jd004073, 2004.

825   Thoning, K. W., Tans, P. P., and Komhyr, W. D.: Atmospheric carbon dioxide at Mauna Loa Observatory: 2. Analysis of the NOAA GMCC data, 1974–1985, Journal of Geophysical Research: Atmospheres, 94, 8549-8565, https://doi.org/10.1029/JD094iD06p08549, 1989.

Tohjima, Y.: Method for measuring changes in the atmospheric O_2/N_2 ratio by a gas chromatograph equipped with a thermal conductivity detector, Journal of Geophysical Research: Atmospheres, 105, 14575-14584, 10.1029/2000jd900057, 2000.

830   Tohjima, Y.: Preparation of gravimetric standards for measurements of atmospheric oxygen and reevaluation of atmospheric oxygen concentration, Journal of Geophysical Research, 110, 10.1029/2004jd005595, 2005.

Tohjima, Y., Mukai, H., Machida, T., Hoshina, Y., and Nakaoka, S. I.: Global carbon budgets estimated from atmospheric O_2/N_2 and CO2 observations in the western Pacific region over a 15-year period, Atmos. Chem. Phys., 19, 9269-9285, 10.5194/acp-19-9269-2019, 2019.

835   Tohjima, Y., Mukai, H., Nojiri, Y., Yamagishi, H., and Machida, T.: Atmospheric O_2/N_2 measurements at two Japanese sites: estimation of global oceanic and land biotic carbon sinks and analysis of the variations in atmospheric potential oxygen (APO), Tellus B, 60, 213-225, https://doi.org/10.1111/j.1600-0889.2007.00334.x, 2008.

Tohjima, Y., Minejima, C., Mukai, H., Machida, T., Yamagishi, H., and Nojiri, Y.: Analysis of seasonality and annual mean distribution of atmospheric potential oxygen (APO) in the Pacific region, Global Biogeochemical
840   Cycles, 26, n/a-n/a, 10.1029/2011gb004110, 2012.

Cucumbers Intercomparison: http://cucumbers.uea.ac.uk/, last access: 24/02/2021.

van der Laan, S., Neubert, R. E. M., and Meijer, H. A. J.: A single gas chromatograph for accurate atmospheric mixing ratio measurements of CO_2, CH_4, N_2O, SF_6 and CO, Atmos. Meas. Tech., 2, 549 - 559, 2009.

van der Laan, S., Karstens, U., Neubert, R. E. M., van der Laan-Luijkx, I. T., and Meijer, H. A. J.: Observation-based
845   estimates of fossil fuel-derived CO_2 emissions in the Netherlands using ^{14}C, CO and [222]Radon, Tellus, 62B, 389 - 402, 2010.

van der Laan-Luijkx, I. T.: Atmospheric oxygen and the global carbon cycle. Observations from the new F3 North Sea platform monitoring station and 6 additional locations in Europe and Siberia, PhD Thesis, Groningen, The Netherlands, 2010.

850   van der Laan-Luijkx, I. T., Karstens, U., Steinbach, J., Gerbig, C., Sirignano, C., Neubert, R. E. M., van der Laan, S., and Meijer, H. A. J.: CO_2, $\delta O_2/N_2$ and APO: observations from the Lutjewad, Mace Head and F3 platform flask sampling network, Atmospheric Chemistry and Physics, 10, 10691-10704, 10.5194/acp-10-10691-2010, 2010.

van der Laan-Luijkx, I. T., van der Laan, S., Uglietti, C., Schibig, M. F., Neubert, R. E. M., Meijer, H. A. J., Brand, W. A., Jordan, A., Richter, J. M., Rother, M., and Leuenberger, M.: Atmospheric CO_2, $\delta(O_2/N_2)$ and $\delta^{13}CO_2$
855   measurements at Jungfraujoch, Switzerland: results from a flask sampling intercomparison program, Atmos. Meas. Tech., 6, https://doi.org/10.5194/amt-6-1805-2013, 2013.

van Leeuwen, C.: Highly precise atmospheric oxygen measurements as a tool to detect leaks of carbon dioxide from Carbon Capture and Storage sites, University of Groningen, Groningen, The Netherlands, 2015.

World Meteorological Organization: 19th WMO/IAEA Meeting on Carbon Dioxide, Other Greenhouse Gases and

860   Related Measurement Techniques (GGMT-2017), World Meteorological Organization (WMO), Switzerland, 2018.

Worthy, D. E. J., Platt, A., Kessler, R., Ernst, M., and Racki, S.: The greenhouse gases measurement program, measurement procedures and data quality, Meteorol. Serv. of Can., Environ. Can., Downsview, Ont., Canada, 97-120, 2003.